Thin–Walled Structures 216 (2025) 113736

Contents lists available at ScienceDirect

Thin-Walled Structures

journal homepage: www.elsevier.com/locate/tws

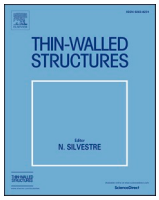

Numerical analysis of hybrid inter-module joints for enhanced seismic resilience of modular buildings

Dan-Adrian Corfar, Konstantinos Daniel Tsavdaridis *

Department of Engineering, School of Science & Technology, City St George's, University of London, EC1V 0HB, London, UK

ARTICLE INFO

Keywords:
Finite element modelling
Hybrid inter-module connections
High-damping rubber bearings
Seismic resilience
Shape memory alloys
Steel modular buildings

ABSTRACT

The seismic resilience of steel modular building systems (MBSs) largely depends on the performance of inter-module connections (IMCs). Conventional IMCs, designed to remain elastic while plastic hinges form in beams, lead to significant residual drifts and permanent damage, limiting module reusability. To address these limitations, this study investigates the cyclic performance of a novel, recently patented, hybrid inter-module connection (HyMC™) and evaluates the influence of key design parameters, such as bolt size, material, and joint stiffness on its seismic behaviour. The connection incorporates a rubber bearing to mitigate damage and enhance post-earthquake functionality. A validated non-linear finite element (FE) model was developed to complement previous experimental work, providing detailed insights into force-transfer mechanisms, stress distribution, and the mechanical behaviour of the connection components. The FE simulations demonstrated strong agreement with experimental results, confirming the effectiveness of the HyMC™ in reducing residual deformations while maintaining structural integrity. The analysis showed that using larger bolt diameters and superelastic SMA studs effectively reduced stress concentrations and permanent deformations, while the addition of joint stiffeners redistributed stresses away from the beam–column zone but increased demands on the bolting assembly, highlighting the need for careful detailing. Future work should further optimise the joint design to enhance re-centring and energy dissipation and extend numerical studies to edge joints. This will support the development of simplified global models to evaluate the effect of the HyMC™ at the building level.

1. Introduction

Modular construction, with origins in ancient prefabrication practices [1], has evolved into the modern volumetric approach prevalent in today's construction industry. Advances in precision manufacturing, automation, and digital modelling have transformed this concept into a highly viable and attractive solution for contemporary building demands. In this approach, three-dimensional (3D) volumetric modules are fabricated in controlled factory conditions and transported to site for rapid assembly [2]. This approach has gained renewed prominence among industry stakeholders and governments seeking to address housing shortages and a diminishing skilled workforce [3], with reported benefits including shortened construction programmes, consistent quality standards, and significant sustainability advantages [4–6].

A key aspect of volumetric modular construction lies in its compatibility with the circular economy ethos, particularly when steel is employed as the primary structural material. Steel's high strength-to-weight ratio, design flexibility, and ease of disassembly through dry, mechanical connections enable steel modular building systems (MBSs) to be repurposed or even fully relocated [7–10]. This extends the service life of modules and reduces overall impact of embodied carbon. However, the expansion of steel MBSs to multi-storey, mid- and high-rise developments has highlighted the critical need for improved seismic resilience, especially in rapidly urbanising regions where growing populations are exposed to hazards such as earthquakes [11–13]. In line with the United Nations Sustainable Development Goals (UN SDGs) [14], improving the seismic resilience of steel MBSs is essential to fully harness the global potential of this technology.

In seismic design, performance-based earthquake engineering (PBEE) [15,16] has shifted the focus from traditional strength-based approaches to frameworks that explicitly consider damage states, residual drifts, and functionality objectives [17–21]. Within steel modular buildings, inter-module connections (IMCs) are pivotal to the global seismic response, governing load transfer between adjacent volumetric modules [22,23]. Experimental studies on inter-module joints (IMJs) under cyclic lateral loads have highlighted the risk of brittle failures in

* Corresponding author.
E-mail address: konstantinos.tsavdaridis@citystgeorges.ac.uk (K.D. Tsavdaridis).

https://doi.org/10.1016/j.tws.2025.113736
Received 26 February 2025; Received in revised form 28 June 2025; Accepted 17 July 2025
Available online 18 July 2025

welds at the intra-module connection when not adequately detailed [24–32]. To mitigate these failures, extensive research has explored IMC details based on capacity-based design principles, with some configurations designed to remain elastic under cyclic loading [30,32–38]. Although these IMCs exhibit energy dissipation capacity and reliable failure mechanisms, they typically rely on plastic hinges forming in the beams of the volumetric modules. Consequently, the resulting residual drifts can be substantial, limiting reparability and impeding the demountability and reuse of the volumetric members.

Alternatively, some studies have explored innovative solutions to improve the seismic performance of the IMCs by incorporating energy-dissipating and self-centring components [39–41]. Building on this concept, Corfar and Tsavdaridis [42] proposed a novel hybrid IMC (HyMC™) system that combines high-damping rubber bearings with superelastic SMA studs. This configuration is the first of its kind to limit damage to the module framing while providing a demountable connection, thereby enhancing residual drift control and post-earthquake functionality, and facilitating disassembly and reuse of modules after a strong earthquake. In the initial study, a proof-of-concept finite element (FE) analysis at the connection level demonstrated promising re-centring and damage control capabilities. This was subsequently confirmed through meso-scale quasi-static cyclic tests at the joint level [43,44], following the FEMA-SAC loading protocol, which validated the hybrid working mechanism of the high-damping rubber and SMA studs and also explored the use of standard high-strength steel bolts as an alternative.

Following the insights gained from the earlier experimental study of the hybrid inter-module connection, a detailed numerical investigation is required to fully capture the complex force-transfer mechanisms and material-level behaviour under cyclic loading, as well as to enable systematic assessment of key design parameters. This paper develops and validates a high-fidelity FE model as an efficient tool for further refining the HyMC™ concept without the high resource demands of repeated experimental testing. The FE analysis serves both to confirm the experimental findings and to extend understanding of the connection's mechanical performance by revealing the evolution of stresses and strains in each component at various stages of cyclic loading.

2. Concept of the proposed hybrid inter-module connection

The HyMC™ system has been developed to provide connectivity between volumetric modules in steel modular buildings. It comprises

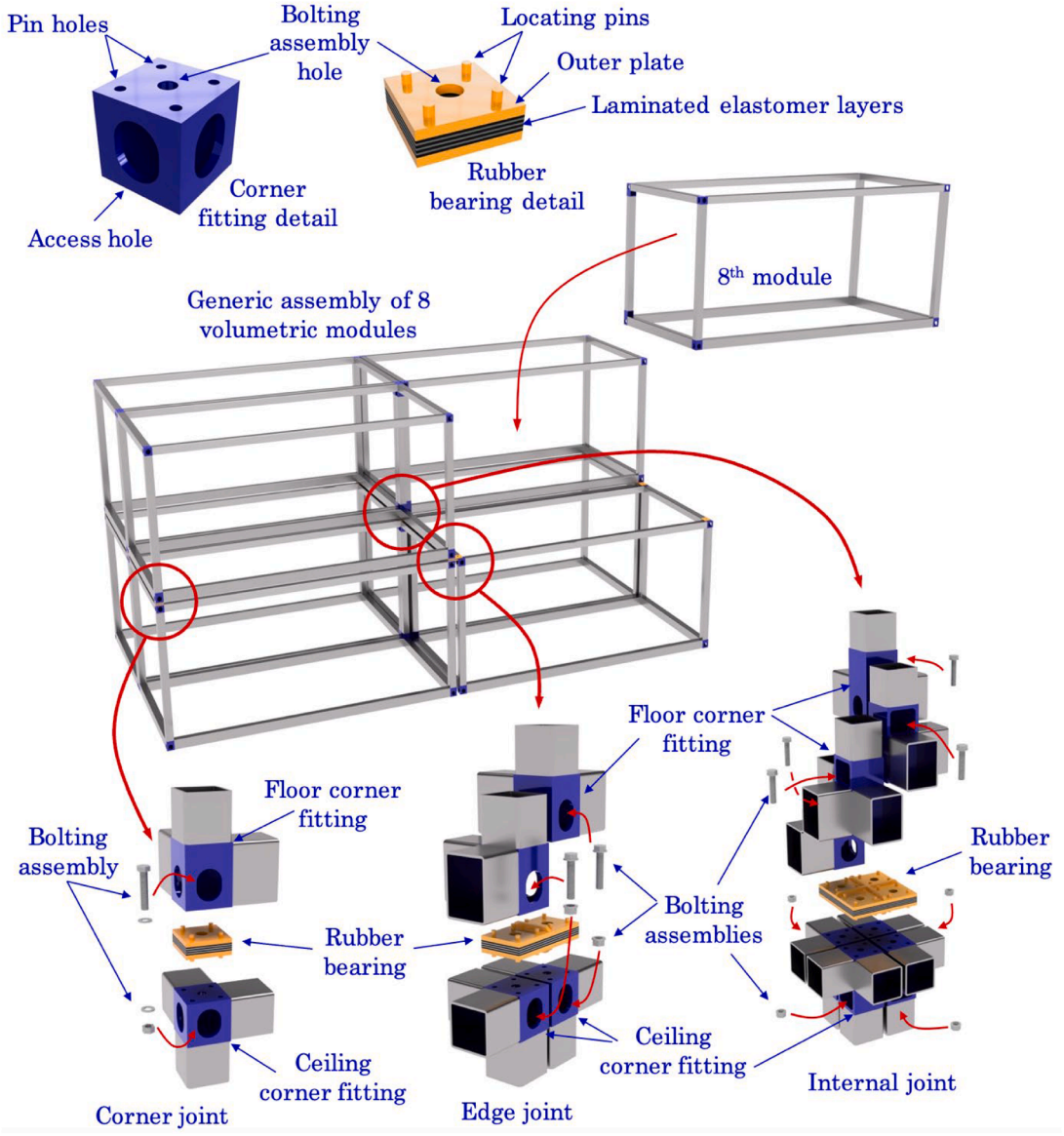

Fig. 1. Concept details of the hybrid IMC.

steel box corner fittings at the module corners, a rubber bearing connector, and a fixing in the form of a bolting assembly. An implementation of the hybrid IMC concept is illustrated in Fig. 1, detailing the connection components and configurations to accommodate corner, edge, and internal joints within a generic assembly of 8 modules.

The steel corner fittings have a square hollow lateral cross-section, designed to match the plan dimensions of the connecting columns and beams of the module's structural chassis. In the current implementation, the fittings form the rigid corners of a typical framed module made of SHS150 columns and ceiling beams and RHS200 × 150 floor beams. The fittings are arranged flush with the external edges of the connecting members to minimise gaps between modules at joints, which could otherwise adversely affect the structure's stiffness. They are also aligned with the columns' centreline to eliminate the unfavourable effect of eccentric loads caused by offsets. Access holes measuring 80 mm × 100 mm with rounded corners (40 mm radius) are provided on two sides of the corner fittings to facilitate the tightening of the bolting assembly. The fitting walls and plates should be sufficiently thick to ensure the corner fittings are stiffer than the connecting members, thus maintaining the structural integrity of the module. For instance, if the section members are 10 mm thick, a 50 % increase in thickness can be assumed when sizing the corner fittings, resulting in 15 mm thick plates.

The rubber bearing connector is sized to match the lateral cross-sectional shape of the corner fittings, with a vertical layout resembling a typical laminated elastomeric bearing, including elastomer layers, reinforcing steel shims, and outer steel plates. As the outer steel plates connect the rubber bearing to the corner fittings, their thickness should be designed to match that of the corner fitting plates. The rubber bearing itself may require customisation in terms of the number and thickness of elastomer layers depending on the specific load requirements and design conditions. This ensures that the structural integrity of the rubber bearing is maintained as a primary means of vertical support for the module corner.

To facilitate positioning of the volumetric modules during installation, the rubber bearing includes guiding lugs (or locating pins) projecting from the outer steel plates, designed to mate with corresponding recesses in the abutting plates of the corner fittings. The diameters of the matching holes are prescribed with a clearance relative to the size of the vertical pins. A 2 mm clearance accommodates typical manufacturing tolerances for the mating parts, while limiting total out-of-verticality by controlling positional errors during installation. To ensure the structural integrity of the pins during assembly, their preliminary size should be proportional to the thickness of the corner fitting plates (e.g., 15 mm diameter pins for 15 mm thick plates). The vertical pins are arranged in a square grid on the rubber bearing outer steel plates to control horizontal misalignment when one module is placed on top of another.

Apertures are provided through the centrelines of the rubber bearing and the abutting corner fitting plates, arranged to form a channel when vertically aligned. The channel is sized to accommodate a bolting assembly, allowing the bottom corner of the upper modules to be coupled to the top corner of the lower modules, with the rubber bearing sandwiched between the fittings. The aperture in the rubber bearing is intentionally larger than those in the abutting corner fitting plates to ensure that the bolting assembly does come into contact with the rubber bearing under horizontal shear deformation. This arrangement provides a number of advantages. Firstly, the centred alignment of the bolting assembly facilitates the design flexibility by providing a simple and symmetric configuration. Secondly, the bolting assembly within the joint is shielded by the corner fitting plates, limiting its direct exposure to flames in the event of a fire and reducing potential damage. Thirdly, as the proposed connection only requires a single bolting assembly to connect adjacent modules at their corners, the assembly and disassembly procedures are streamlined in modular buildings with a large number of connection points.

An example installation sequence for two modules coupled using the proposed connection was illustrated in Fig. 2. In the first two steps, the lower module is installed, followed by the rubber bearings which are inserted into the fittings at each module corner using the vertical pins as guide. In the third step, the upper module is lifted and positioned on top of the lower module, lowered onto the rubber bearings, and aligned using the locating pins on the rubber bearings' top plates for a smooth plug-in motion. Finally, the vertical connection between the stacked modules is secured by installing the bolting assemblies. For corner and external joints, the bolting assemblies can be inserted through the access holes in the corner fittings. For internal joints, corner fittings may be extended to allow access for bolt tightening, avoiding the need to

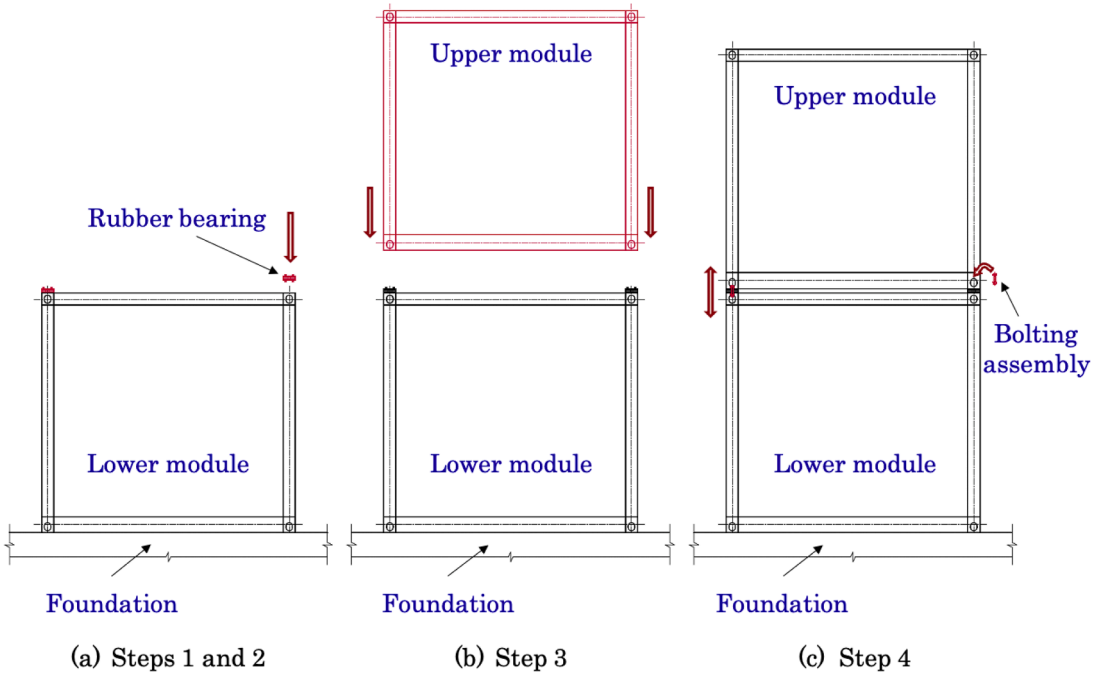

Fig. 2. Suggested installation sequence.

weaken the module frame members by cutting holes into the section walls. Alternatively, parallel flange channel (PFC) sections can be used for the beams, oriented with the cavity facing inward and flush with the outline of the corner fittings, which would be inverted. This configuration positions the access holes inside the module, enabling connection assembly at internal joints without extending the corner fittings. In some cases, an alternative approach could involve eliminating bolts at internal joints altogether, instead relying solely on the bearings and shear keys, as significant tensile forces are not typically expected in these locations. In practice, for fully prefabricated modules with enclosed finishes, small, concealed latch doors can be provided to allow access for bolt tightening where needed. The connections should be positioned in non-intrusive locations, ideally in corridors or service areas, to avoid interference with doorways, windows, and interior finishes.

While the installation procedure is straightforward and demonstrates the assembly-friendly design of the proposed hybrid IMC, some practical considerations remain. For example, working at height is required to install the bolting assemblies, which should be addressed in the method statement and risk assessment for each project. Additionally, the presence of rubber bearings necessitates careful planning of the staged construction process to accurately predict compression in the rubber layers as the building is erected.

2.1. Working mechanism

The proposed connection is designed to provide both vertical and horizontal connectivity between modules, with each connection component essential for different loading scenarios. For the case of vertical connectivity, the main force-transfer mechanisms are illustrated in Fig. 3.

Under the action of permanent and variable gravitational loads, axial compression (Fig. 3 (a)) is resisted by the rubber bearing, which provides even and continuous vertical load paths between the upper and lower module corner fittings. As an almost incompressible material subjected to a compression force, the sides of the rubber layers are expected to bulge as the top bearing plate displaces vertically downwards. The level of vertical displacement can be controlled during design by adding reinforcing steel plates to reduce the thickness of the individual elastomer layer without affecting the horizontal stiffness.

For combinations of actions including lateral loads such as those from wind or earthquake, most IMCs are subjected to horizontal shear forces as shown in Fig. 3 (b). Under this load case, the resilience of the rubber bearing is critical, as it accommodates the inter-storey shear forces by undergoing large shear deformations without failing. In this regard, the use of a high-damping rubber compound is highly desirable as provides a bespoke mechanical response based on the level of shear strain reached. The shear stiffness of high-damping rubber is higher than that of regular, low-damping rubber at small strains, ensuring that the

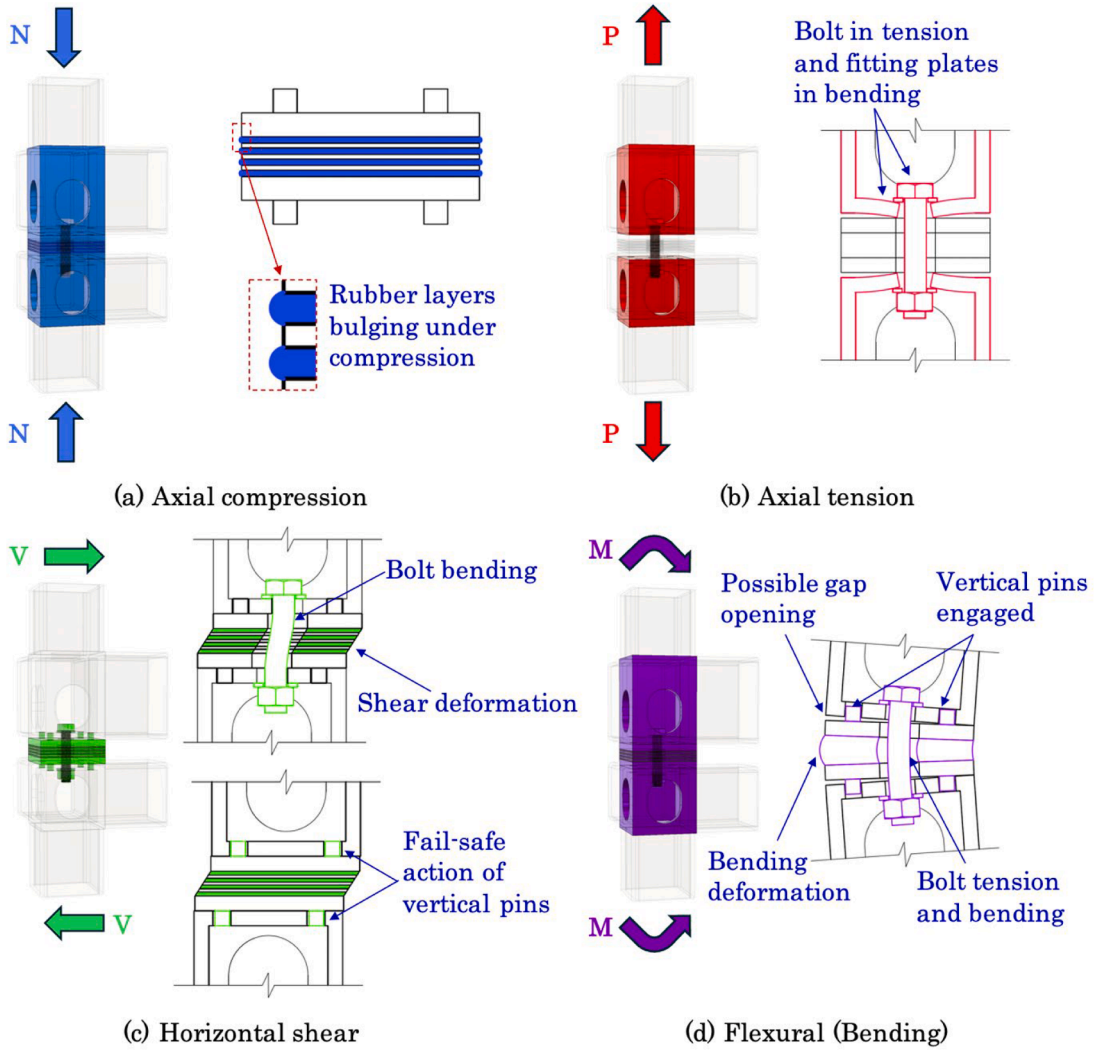

Fig. 3. Possible force-transfer mechanisms in the hybrid IMC for a vertical connection.

IMC is not easily excited under small loading caused by wind or low-intensity earthquakes. With increasing strains, the stiffness decreases, initiating a hybrid working mechanism as the bolting assembly is engaged in bending between the upper and lower corner fitting bolt holes, contributing to the overall shear resistance of the IMC. At larger strains, the shear stiffness of high-damping rubber increases again, providing a fail-safe action, while in more onerous load cases which may cause a total failure of the bolt, the vertical pins provide a further means of fail-safe action, preventing the modules from accidentally topping off of the rubber bearings.

Consequently, an envisaged implementation of the proposed hybrid IMC includes a bolting assembly made of superelastic SMA, which is intended to limit the permanent bending deformation of the shank by virtue of the shape recovery property of SMAs. Such a behaviour would be favourable for reducing the residual drifts to facilitate the connection demountability even in the aftermath of strong winds or major earthquakes, as opposed to HSS steel bolts which may deform to such an extent as to become jammed in the connection.

In some cases, the uppermost floors in high-rise modular buildings may experience uplift as the structure behaves like a vertical cantilever under lateral loads. In such scenarios, the bolting assembly is crucial for resisting the resulting tension force in the hybrid IMC, as shown in Fig. 3 (c). On the other hand, in the absence of lateral loads, the bolting assembly is also essential for ensuring robustness, providing the necessary tying action between modules during extreme loading events that may cause a loss of support.

Accordingly, the preliminary design of the hybrid IMC at a corner joint should adopt a minimum bolt size of M16. This recommendation is based on a minimum tying force of 50 kN for a typical corner supported steel modules with a self-weight up to 6 kN/m^2, as specified by Lawson et al. [2], while assuming an ultimate tensile strength of 800 N/mm^2 for class 8.8 bolts, in accordance with Eurocode 3, Part 1–8 [45]. While the final bolt diameter will be determined by the bending resistance required to resist the horizontal shear forces and control inter-storey drift, it is important to note that the upper bolt diameter limit is constrained by constructional considerations. Specifically, the tools needed to tighten the bolt (e.g., spanner/torque wrench, socket heads, adapters) must fit within the access hole of the corner fitting.

Another force-transfer mechanism for the vertical connection is pure bending of the hybrid IMC, as shown in Fig. 3 (d). In this scenario, the flexural rigidity of the IMC would be relatively low, equivalent to a pinned connection. The centred alignment of the bolt provides a limited

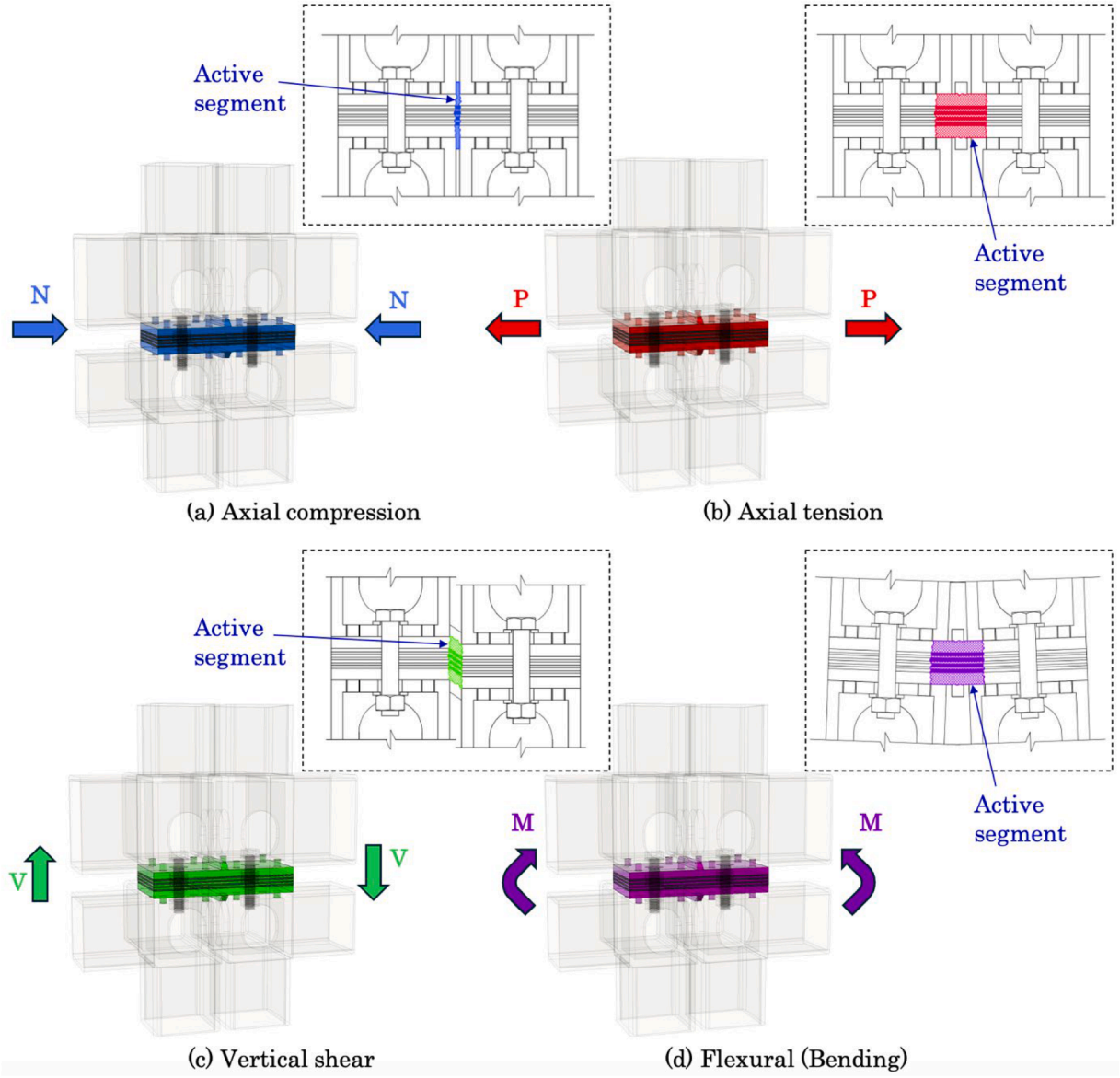

Fig. 4. Possible force-transfer mechanisms in the hybrid IMC for a horizontal connection.

lever arm to counteract the joint's flexure, potentially leading to gaps between the corner fittings and the rubber bearing.

However, this type of loading is less likely to occur in a modular building under typical loading scenarios. The volumetric modules are expected to behave as rigid box-like frames due to rigid connections between the ceiling and floor beams and the corner posts, which prevent excessive rotational deformations at the module corners.

Fig. 4 shows the primary force-transfer mechanisms envisaged for horizontal connectivity at an edge joint equipped with the hybrid IMC. In this configuration, the rubber bearing serves as the main functional component, providing the necessary resistances to compression, tension, shear, and bending through the respective active segments highlighted in Fig. 4. The corresponding resistances of the horizontal connection are therefore governed by the cross-sectional properties of the rubber bearing component, with preliminary sizing potentially simplified by ignoring the contribution of the rubber layers. Due to the multiple steel plates within the rubber bearing component, the horizontal connection is expected to be stronger and stiffer than a typical gusset or side plate. Consequently, the horizontal connection can reasonably be assumed to exhibit a rigid, elastic behaviour for the purposes of simplified joint modelling for global analysis.

2.2. Special considerations for the hybrid IMC

2.2.1. The gap between modules and fire safety

Recent studies have investigated the potential benefits of eliminating the horizontal gap between modules to create composite action between ceiling and floor beams [46–49]. However, the gap introduced by the rubber bearing is deemed beneficial for the structural flexibility of volumetric modules. Designing floor and ceiling beams to span independently between corner columns allows future repurposing or relocation of individual modules if architectural layout changes are desired during the steel modular building's life cycle. This design approach also facilitates lifting and moving the modules, enhancing their versatility and ease of handling during transportation or reconfiguration. Moreover, the air barrier enhances the acoustic performance of the modular structure by reducing sound transmission [50].

The gap between modules also raises fire safety concerns, particularly regarding the sensitivity of the rubber bearings to fire compared to typical seismic isolators located at the base of structures. In this regard, it should be mentioned that the rubber bearings benefit from the implicit fire safety measures specific for modular buildings. Modules are effectively isolated from each other by fire protection layers, typically made of plasterboard, and additional fire stoppers are installed in cavities to prevent the rapid spread of fire through the air gaps between modules [2]. These measures effectively mitigate the risk of damage to rubber bearings in the event of a fire.

2.2.2. Cost implications and connection repeatability

The inclusion of rubber parts in the hybrid IMC includes cost implications compared to simpler bolted or welded connections. Fabrication costs for rubber bearings should be considered alongside with potential offsets from mitigating module damage during an earthquake, maintaining asset value for future reuse, and improving repairability. Moreover, as the building height increases, the cost impact of connection duplication also rises. To optimise material use, the connection configuration must meet specific performance design constraints at each floor level. The impact of connection repeatability may also be lowered by determining whether the developed solution is needed only at specific levels along the building height to achieve a desirable global response. This should be assessed by global analysis, considering all relevant parameters such as site location, building height, or earthquake intensity.

In addition to the rubber bearings, the use of superelastic shape-memory alloy (SMA) studs also affects the overall cost of the hybrid connection. The relatively high manufacturing cost of commercially available Nickel-Titanium (Ni-Ti) parts must be accounted for, although this can be justified by the gains in residual drift control, enhanced demountability, and reusability, as SMA studs recover their original shape after deformation. Meanwhile, advancements in manufacturing technologies, including additive manufacturing techniques such as selective laser melting (SLM) or direct energy deposition (DED), are expected to reduce future manufacturing costs for Ni-Ti parts [51–53]. Alternatively, iron-based SMAs (Fe-SMAs) could be used for the bolting assembly. Widely recognised for their improved low-cycle fatigue resistance compared Ni-Ti-based SMAs, Fe-SMAs are also cheaper and easier to manufacture due to their composition [54]. However, since Fe-SMAs do not provide the same level of shape recovery and residual deformation control, further investigation is needed to assess their suitability for the proposed hybrid IMC.

3. Validation of the numerical model of the hybrid inter-module joints

The finite element (FE) models of the hybrid IMJs were developed in Abaqus [55] based on the meso-scale cyclic tests by Corfar and Tsavdaridis [43].

Fig. 5 shows a diagram of the test frame and its loading system, designed to simulate the appropriate support conditions for the IMJ prototypes under the effect of bi-axial loading applied to the top column, according to the J/C test setup for unbraced modular frames subjected to lateral load [56]. The tests were carried out according to the ANSI/AISC 341–22 [57] recommendations, while the displacement-controlled standard FEMA/SAC [58] loading sequence was applied through the horizontal actuators in a quasi-static manner at a rate of 10mm/min to limit the influence of dynamic effects. To capture the effect of gravitational actions, an axial load equivalent to 5 % of the compressive yield capacity of the 150 × 150 × 8 SHS post and 4.7 MPa compressive stress on rubber bearing was kept constant throughout the test.

3.1. Material models

3.1.1. Structural steel

Structural steel was defined by a bi-linear model with kinematic hardening and plasticity based on the Von Mises yield criterion. The material properties for the frame members were derived from the tensile coupon tests (Table 1). For the corner fittings, stiffeners, outer steel plates, and the steel shims within the rubber bearings, nominal material properties corresponding to S355 grade steel were assumed in accordance with Eurocode 3, Part 1–1 [59]. Similarly, the high-strength steel for the class 8.8 bolting assemblies was based on nominal properties provided in Eurocode 3, Part 1–8 [45].

3.1.2. High-damping rubber

In order to describe the large-strain and highly non-linear mechanical behaviour of the high-damping rubber vulcanizate, the constitutive material model for rubber has been defined using the Bergström–Boyce (BB) hysteresis model, based on Yeoh hyperelasticity.

The calibrated stress-strain response was illustrated in Fig. 6. The comparison with the engineering stress-strain curve from the double bonded shear (DBS) test demonstrated the accuracy of the BB–Yeoh model in capturing the HDR's typical S-shaped stress-strain behaviour as well as the pronounced hysteresis over the desired strain range.

The resulting material parameters adopted in the FE model were summarised in Table 2. To approximate the fully incompressible behaviour of elastomers, the solver required that the D_i terms defining material compressibility be taken as zero. For additional insights into the material model calibration process, the background on the hyperelasticity class of constitutive models, as well as other forms of the strain energy function considered during the calibration study, refer to Corfar and Tsavdaridis [42].

The simplified FE model of the DBS test illustrated in Fig. 7 was

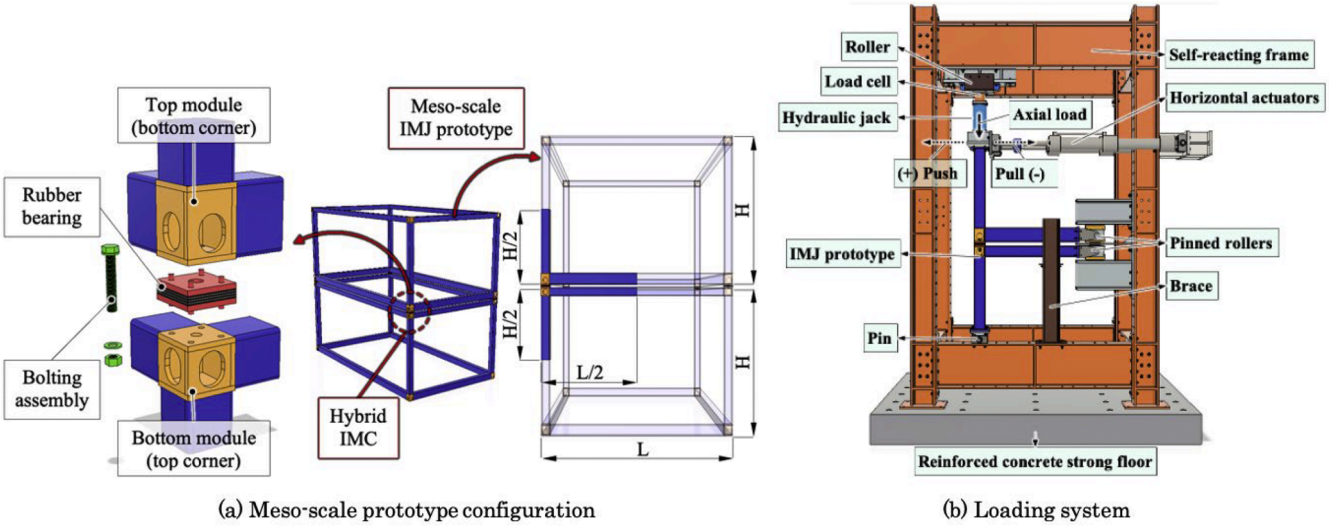

Fig. 5. Details of the cyclic tests on hybrid inter-module joints (adapted from [44]).

Table 1
Material properties of structural steel.

Frame member	Steel grade	Young's modulus	Yield strength	Ultimate tensile strength
Top post	S355J2H	209 GPa	505 N/mm^2	546 N/mm^2
Bottom post	S355J2H	205 GPa	438 N/mm^2	496 N/mm^2
Floor beam	S355J2H	190 GPa	433 N/mm^2	507 N/mm^2
Ceiling beam	S355J2H	202 GPa	541 N/mm^2	565 N/mm^2

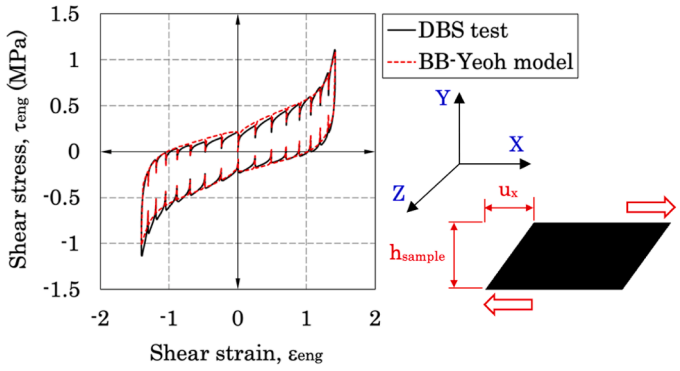

Fig. 6. Material calibration of the BB-Yeoh model for rubber.

adopted to check the validity of the calibrated BB-Yeoh model. The simple shear loading mode was imposed on a cylindrical rubber strip by fixing the bottom surface and applying two displacement-controlled cycles of up to ±200 % shear strain (12 mm horizontal displacement) at the top. The displacement was applied to a reference point connected to the top surface through kinematic coupling, while the symmetric configuration of the DBS test allowed for only half of the cylindrical rubber strip to be modelled by using the symmetrical boundary conditions. The hysteretic loops illustrated in Fig. 7 demonstrated a good agreement between the FE prediction and the DBS test, capturing the non-linear S-shaped load-displacement curve as well as the pronounced hysteresis of high-damping rubber.

3.1.3. *Superelastic shape memory alloy*

In Abaqus, the uniaxial flag-shaped stress-strain response of phase transforming materials such as austenitic SMAs can be modelled by the superelasticity model developed by Auricchio and Taylor [60,61]. The superelasticity model is intended for modelling Ni-Ti based SMAs that undergo solid-solid, martensitic phase transformation defined by the stress-strain curve shown in Fig. 8, capturing the closed hysteresis loop with large recoverable deformations during load-unload cycles at finite strains.

The superelasticity model has been widely adopted for modelling self-centring structural systems using SMA components with reasonable accuracy [62–68].

In this study, the superelastic model was calibrated based on data from the first cycle of a uniaxial tensile test presented in [42]. To facilitate the calibration process, a simplified FE model of the test was adopted (Fig. 9). The loading conditions of the cyclic uniaxial tension test were imposed by means of reference points connected to the outer surfaces of the coupon ends using kinematic coupling. The resulting stress-strain response (Fig. 9) showed a good match with the experimental data, supporting the validity of the calibrated superelastic model. The corresponding material parameters were given in Table 3.

3.2. *Geometry and loading*

Fig. 10 shows details of the FE models, including constraints,

Table 2
Material properties for high-damping rubber.

Hyperelasticity coefficients (Yeoh model)						Hysteresis (Bergström-Boyce model)			
C_{10}	C_{20}	C_{30}	D_1	D_2	D_3	S	A	m	C
0.139	-0.014	0.003	0	0	0	24.7	141.4	10.85	-0.99

Note: (1) C_{i0} are stiffness coefficients, (2) D_i are compressibility coefficients, (3) S is a stress scaling factor, (4) A is the creep parameter, (5) m is the effective stress exponent, (6) C is the creep strain exponent.

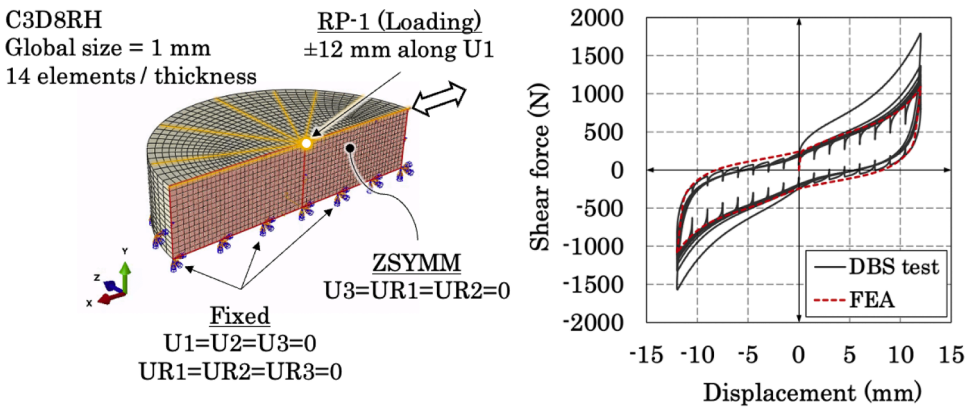

Fig. 7. Finite element model of the DBS test.

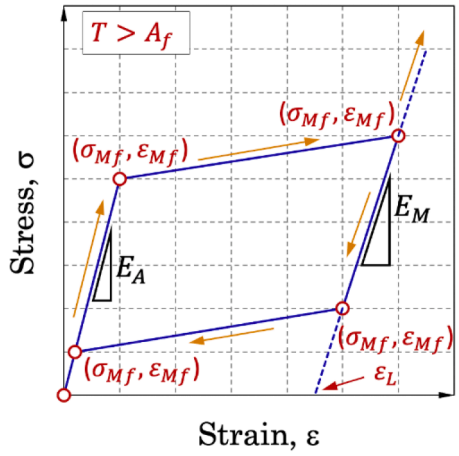

Fig. 8. Constitutive model for the superelastic SMA.

boundary conditions, applied loads, and meshing controls.

The FE models focused on the influence of six parameters on the mechanical behaviour of the hybrid inter-module joint (IMJ) prototypes. Specifically, two sizes of austenitic shape-memory alloy (SMA) studs were considered to assess whether the nonlinearity associated with the superelastic Ni-Ti alloy's phase transformation significantly affects the joints' re-centring and energy dissipation capacity. High-strength steel bolts were also used to provide a direct comparison with the SMA studs, highlighting the effect of bolt size and material strength on the connection's working mechanism. Additionally, two beam–column joint details were included to investigate the role of intra-module connection stiffness at the joint level. The parameters for each model are listed in Table 4 and illustrated in Fig. 11.

To enhance computational efficiency, the symmetry of the test configuration was leveraged by modelling only half of the specimen. The nuts, washers and bolt rod were modelled as a single part. The welded connections between the hollow members and the corner fittings were modelled using surface-to-surface "Tie" constraints, while the reference points at the members' ends were connected to the specimens using kinematic coupling constraints. An ideal steel–rubber bond was assumed for the rubber bearing by merging its components (outer steel plates, steel shims, and elastomer layers) into a single part while preserving geometric boundaries and material properties. This approach reduces computational cost by avoiding numerous contact definitions.

Table 3
Parameters for the superelastic material model.

Property	Value
Young's modulus of austenite, E_A	87,500 MPa
Young's modulus of martensite, E_M	38,438 MPa
Poisson's ratio of austenite, ν_A	0.33
Poisson's ratio of martensite, ν_M	0.33
Forward transformation start stress, σ_{Ms}	525 MPa
Forward transformation finish stress, σ_{Mf}	615 MPa
Reverse transformation start stress, σ_{As}	180 MPa
Reverse transformation finish stress, σ_{Af}	90 MPa
Total transformation strain, ε_L	3.64 %

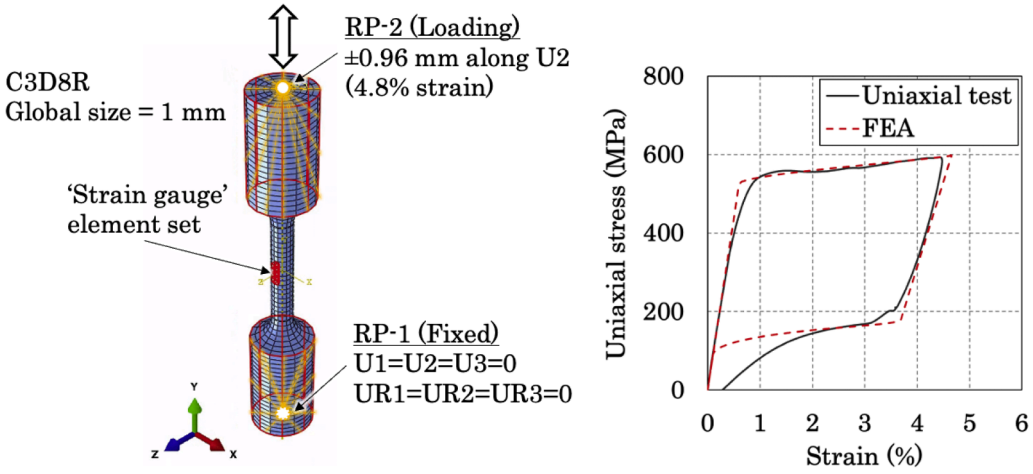

Fig. 9. FE model of the uniaxial tensile test for the Ni-Ti coupon.

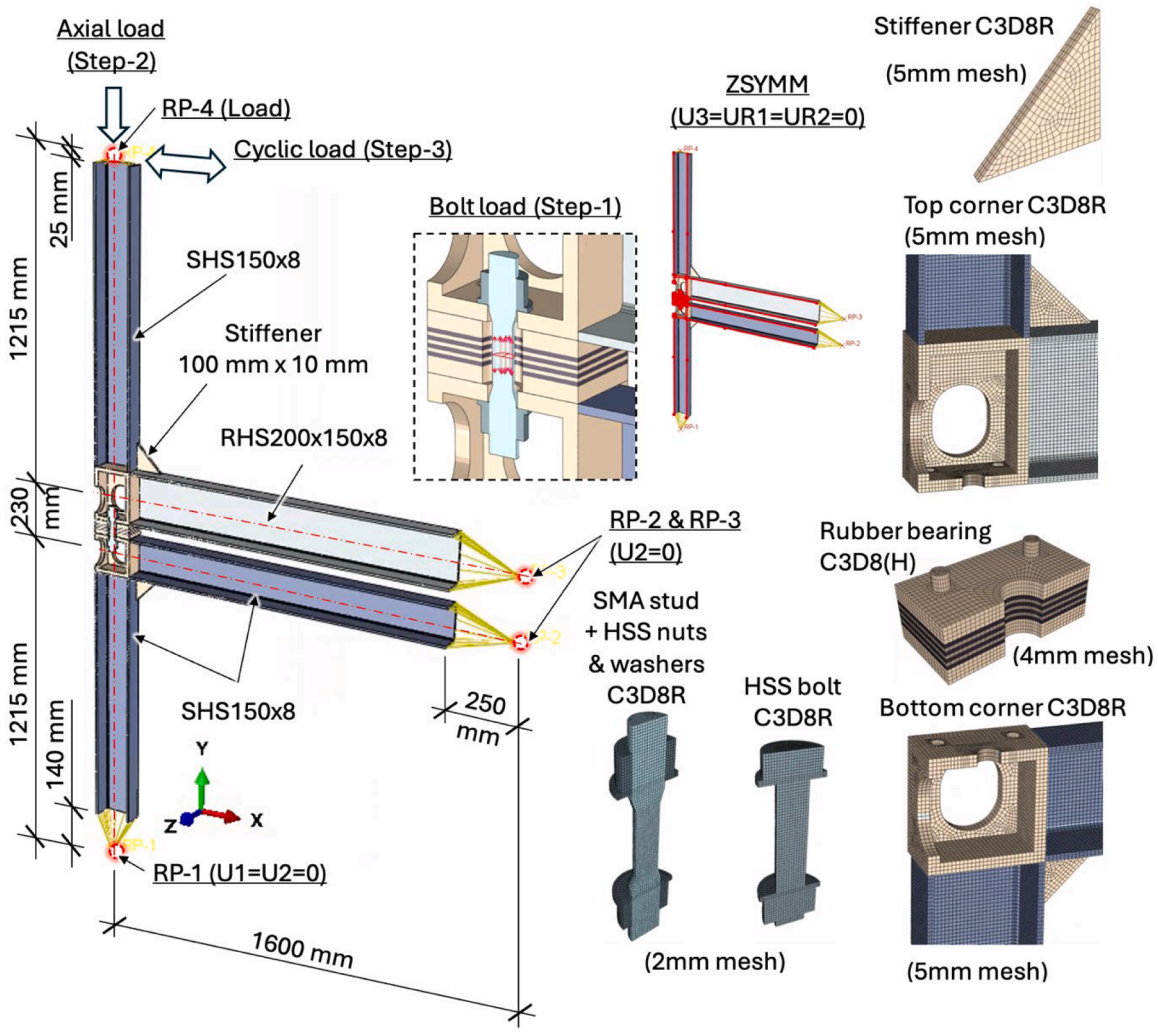

Fig. 10. Overview of the FE models.

Table 4
Summary of parameters considered in the FE models.

Joint prototype	Bolting assembly	Beam-column joint
IMJ01	M20–27* SMA stud	Unstiffened
IMJ02	M20–27 SMA stud	Stiffened
IMJ03	M16–24* SMA stud	Unstiffened
IMJ04	M24, class 8.8 bolt	Unstiffened
IMJ05	M24, class 8.8 bolt	Stiffened
IMJ06	M27, class 8.8 bolt	Stiffened

* Note: M20–27 and M16–24 indicate double-end threaded SMA studs with a reduced internal shank diameter of 20 mm or 16 mm, respectively, and M27 or M24 threaded ends, forming a dog-bone profile.

Surface-to-surface contact pairs with small sliding formulation were defined between the rubber bearing outer steel plates and the corner fitting abutting plates, as well as between the bolting assembly and the corner fittings. "Hard" contact was enforced in the normal direction, with the default penalty friction formulation applied in the tangential direction. Following extensive trials, a friction coefficient of 0.2 was determined for the contact between the rubber bearing and the corner fittings. A friction coefficient of 0.05 was assumed for contact between all bolt assemblies and the corner fitting plates to replicate the slip condition observed during testing, where the loss of initial hand-tightening pretension resulted in bolt movement within the clearance of the bolt holes.

The FE models included three general static analysis steps: bolt tightening, axial load, and the cyclic lateral load protocol. Because only half of the specimen was modelled, the magnitude of the applied loads was also halved, while this had to be accounted for in the results by multiplying the reaction forces by two. Therefore, to simulate the initial snug-tight condition, a 10 kN bolt load was applied, which was then reduced to 1 kN during the axial load step to replicate the loss of preload due to the vertical displacement of the rubber bearing. This reduction still ensured a minimal level of contact between the washers and the corner fittings to aid convergence. The magnitude of the bolt load was then fixed during the cyclic load step. In the second step, a 50 kN axial load was applied, followed by a truncated cyclic load protocol (Table 5) that included a single cycle at each drift ratio level to enhance computational efficiency. Since the tests showed no significant degradation in the hysteretic behaviour of the IMJs over repeated cycles, this approach was considered a satisfactory trade-off between computational time and validation accuracy, ensuring the FE model can accurately capture peak responses, deformation, failure modes, and overall force transfer mechanisms at each drift ratio level, while minimising computational demands.

All steel parts were modelled using first-order 8-node linear brick (3D solid) elements (C3D8R) with reduced integration and hourglass control, while fully integrated first-order 8-node hybrid linear brick elements (C3D8H) were employed for the rubber layers. To increase the accuracy of the stress contours, a finely meshed region was defined, which included the connection parts and 400 mm segments (twice the

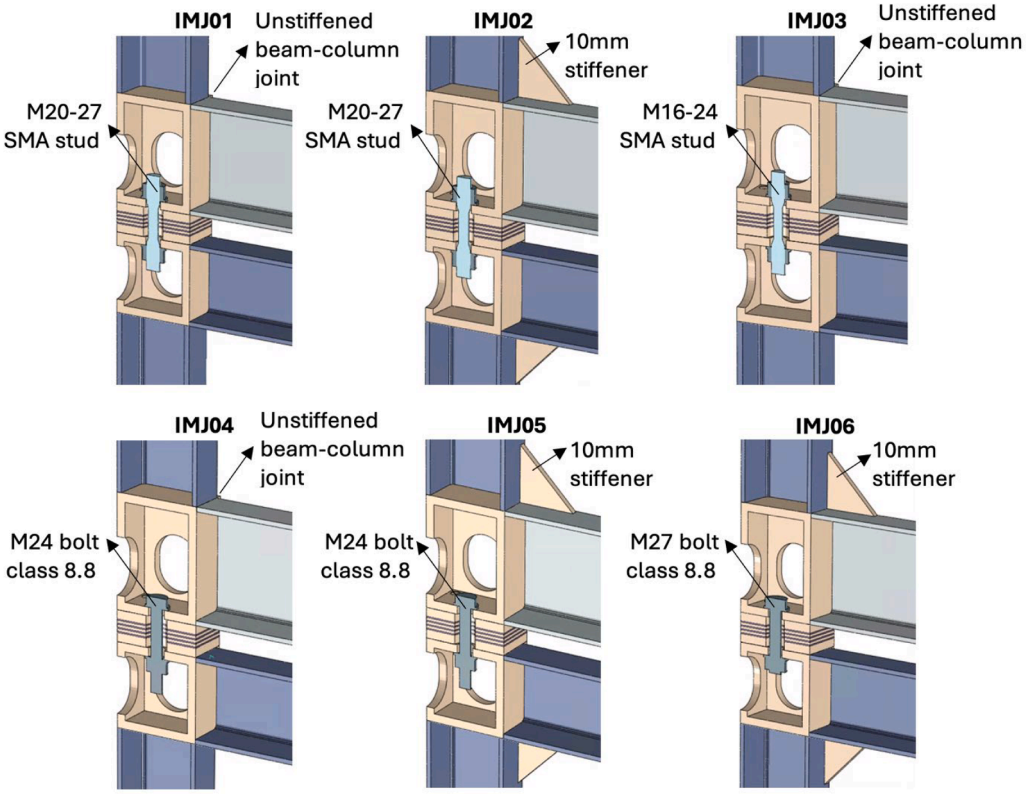

Fig. 11. Summary of the six FE models.

Table 5
Truncated cyclic test protocol based on FEMA/SAC loading history.

Loading stage	Inter-storey drift ratio	Applied lateral displacement	Number of cycles
1	0.375 %	10.3 mm	1
2	0.5 %	13.8 mm	1
3	0.75 %	20.6 mm	1
4	1 %	27.5 mm	1
5	1.5 %	41.3 mm	1
6	2 %	55 mm	1
7	3 %	82.5 mm	1
8	4 %	110 mm	1

floor beam depth) near the beam-column joint zone. The mesh element size for the corner fittings and frame members within the IMC region was set to 5 mm, the bolting assembly to 2 mm, and the rubber bearing to 4 mm. Outside the IMC region, the mesh element size for the frame members varied between 10 mm and 100 mm. Following well-established recommendations in the literature, a minimum of three mesh elements was ensured through the thickness of the hollow section walls to accurately capture stress and strain gradients under bending and shear. To balance computational effort and accuracy, the rubber layers were modelled with five mesh elements through their thickness, which was sufficient to accurately capture the bulging effect of the rubber under compression. The 3mm-thick steel shims similarly modelled with three mesh elements through their thickness. A visual representation of the meshed parts was shown in Fig. 10.

3.3. Validation study

The FE models were validated by experimental test data from the reference study [43]. Fig. 12 presents a comparison of the hysteresis loops from both the tests and FEA, demonstrating a strong correlation in terms of stiffness and strength in both loading directions. The FE models accurately predicted the reduced strength of specimen IMJ04 during reverse loading at a 4 % drift ratio, as well as the enhanced stiffness and lateral load capacity of the specimens with stiffened beam-column joints and larger bolt diameters. Fig. 13 shows a direct comparison of the observed failure modes for IMJ04, confirming the validity of the stress and strain distributions predicted by the FE model. Specifically, the FEA identified high stress concentrations at the intra-module connection (Fig. 13 (a)), consistent with the weld cracking observed experimentally at −4 % drift ratio, with predicted stresses exceeding the nominal ultimate tensile strength of S355 steel. Similarly, the predicted plastic strain distribution in the bolt shank Fig. 13 (b) matches the deformed shape and thread damage observed in the tested specimen after the cyclic loading protocol.

While there are some isolated differences between the FEA results and the experimental tests, further refinement of the FE models is constrained by the unpredictable movement of the bolt during testing, which introduces uncertainties that are difficult to model accurately. Therefore, to improve the FEA validation, the design of the hybrid IMC connection must be optimised to achieve more controllable bolt behaviour. Nevertheless, the overall findings confirm the FE model's capability to accurately simulate the hysteretic behaviour of hybrid IMJs under cyclic lateral loading. This validation supports the reliability of the FE model for further analysis, providing deeper insights into the stress and strain states of each connection part, which were not fully captured during the tests.

4. Insights into the behaviour of the hybrid IMC from FEA

4.1. Stress and strain development in the connection components

Figs. 14 and 15 illustrate the Von Mises stress distribution at the maximum drift ratio achieved in each direction for the specimens equipped with shape memory alloy (SMA) studs and high-strength steel (HSS) bolts, respectively. The stress contours reflect the anticipated

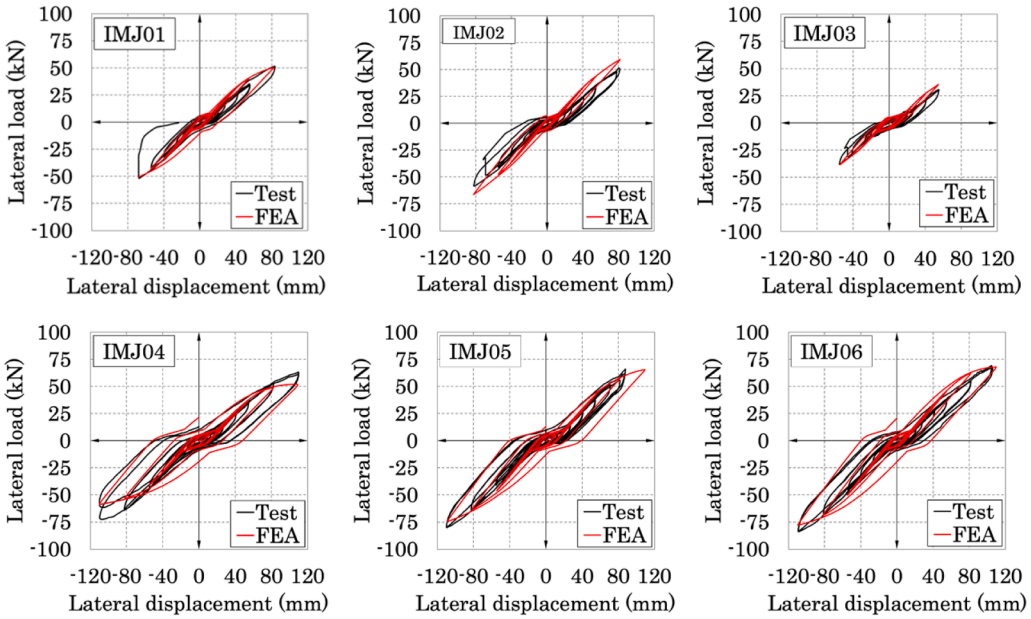

Fig. 12. Tests vs. FEA hysteresis loops.

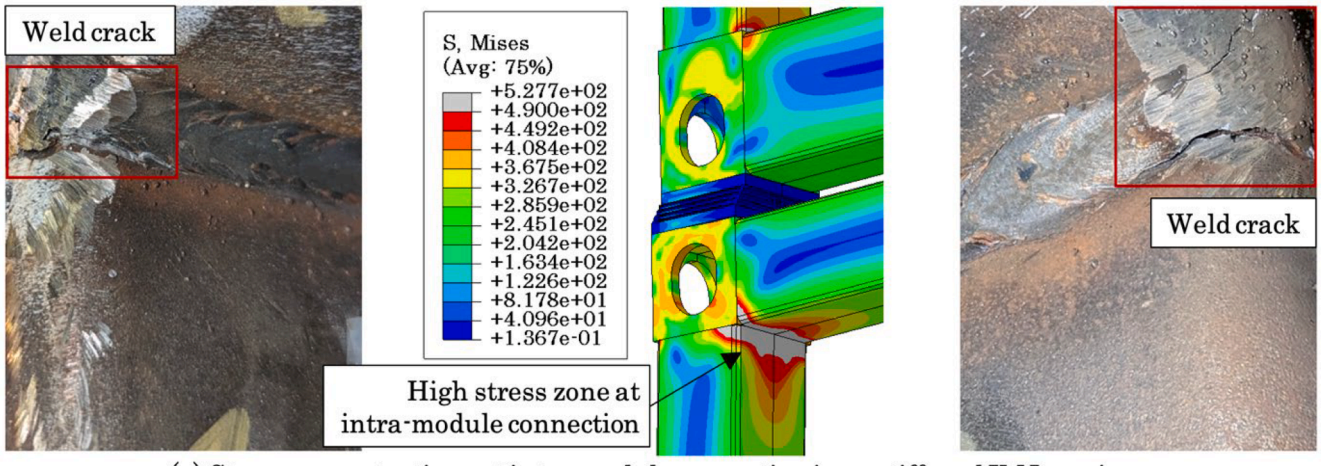

(a) Stress concentrations at intra-module connection in unstiffened IMJ specimen

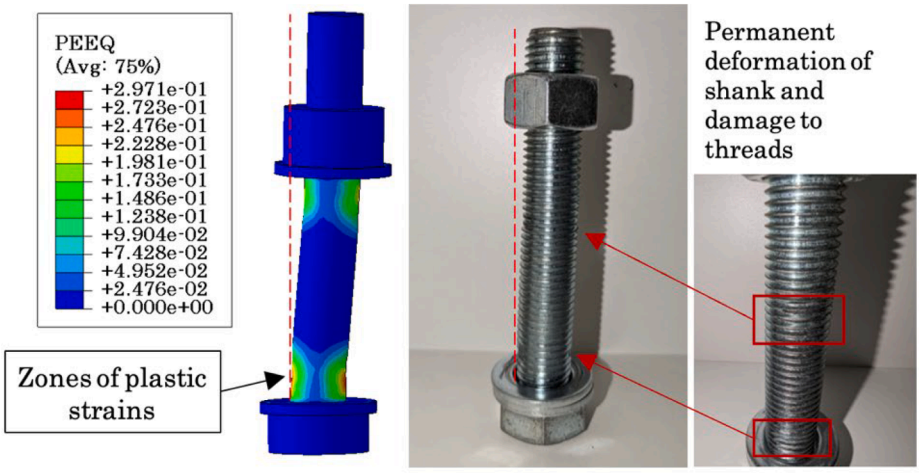

(b) State of deformation and plastic strains in M24 bolt at end of loading protocol

Fig. 13. Comparison of test and FEA failure modes for unstiffened specimen IMJ04 with M24 class 8.8 bolt.

force-transfer mechanisms characterised by the flexural bending of the joint members, with tensile and compressive stresses developing in the walls of the hollow sections perpendicular to the loading direction. Generally, the six specimens exhibited similar stress distributions, with specific differences in the stress levels at the intra-module connections, near the stiffeners, and within the shank of the bolting assemblies.

The FE models accurately captured the stress concentrations at the intra-module connections near the beam-column joint zone,

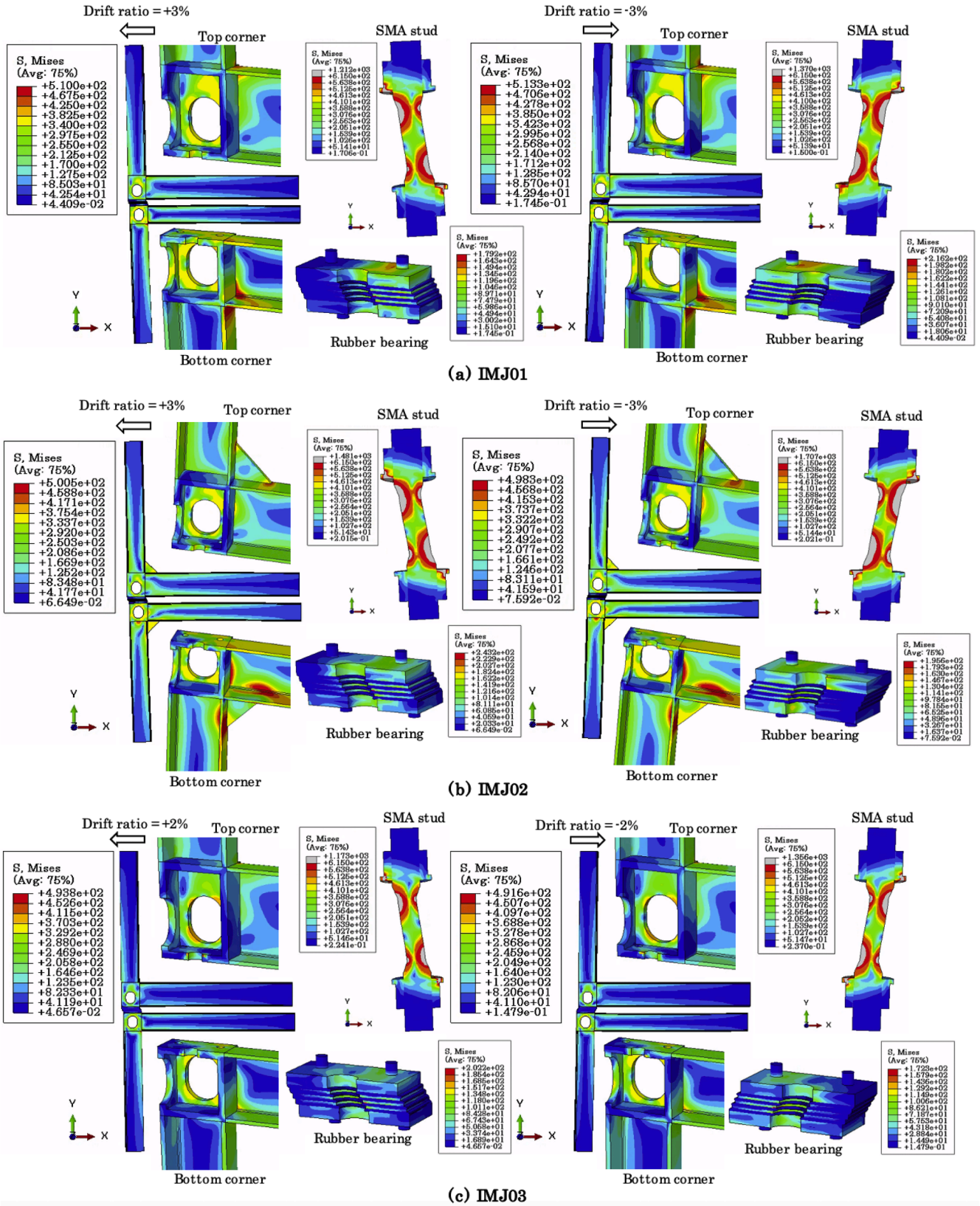

Fig. 14. Deformation and Von Mises stress distribution of the hybrid IMJs with SMA studs.

corresponding to the weak regions that failed by weld cracking in specimen IMJ04, as previously reported [43]. It was also observed that specimens with stiffened intra-module connections demonstrated different force-transfer mechanisms. Specifically, the triangular stiffeners shifted the highly stressed regions away from the corners near the beam-column joints, reducing the stresses in these regions. FEA results further confirmed that adding stiffeners at the intra-module connections increases the stresses in the bolting assemblies as shown in

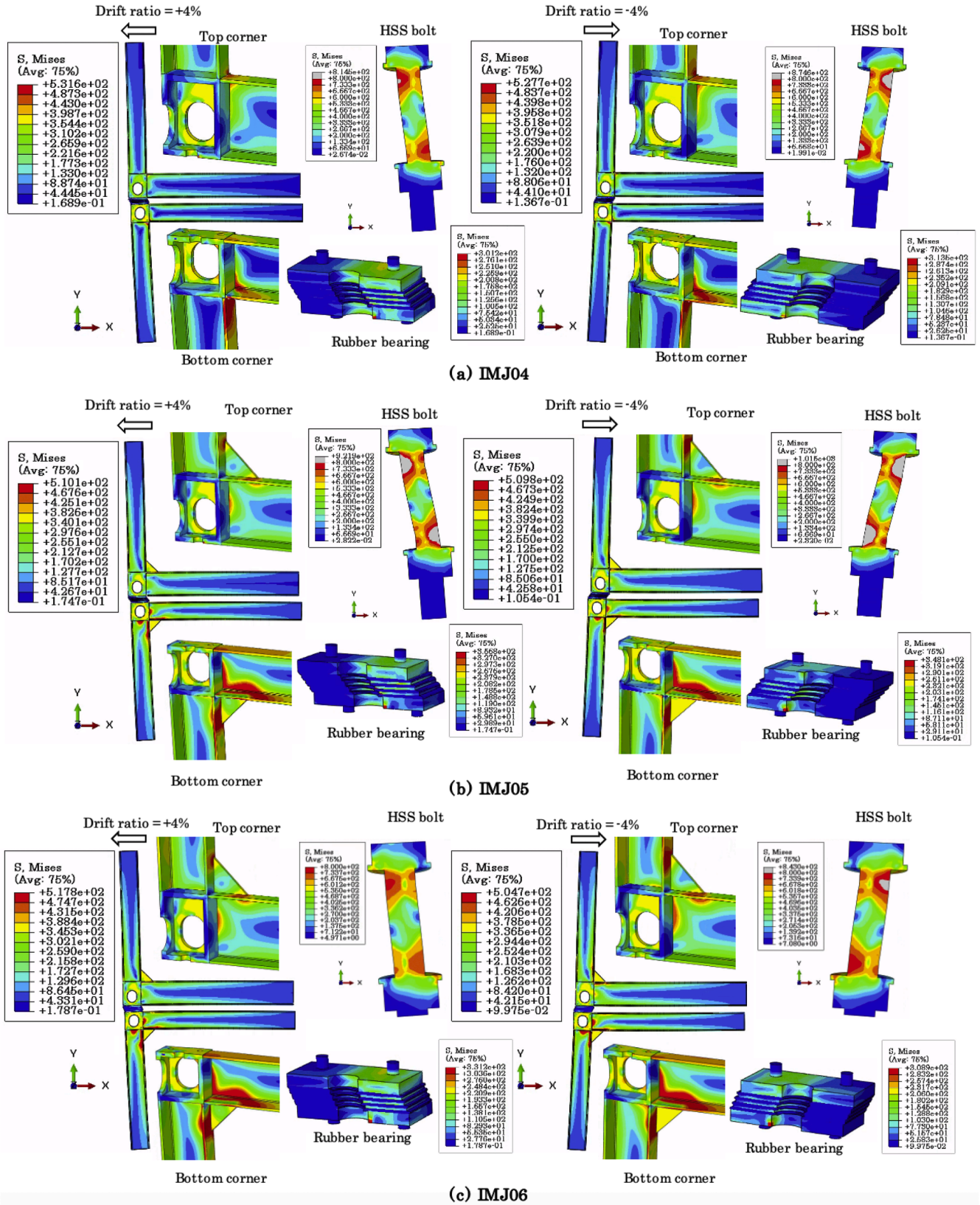

Fig. 15. Deformation and Von Mises stress distribution of the hybrid IMJs with HSS bolts.

Figs. 14 (a)-(b) and 15 (a)-(b). Conversely Fig. 15 (c) demonstrated that increasing the bolt size can help reduce the stresses developed in the bolts.

Overall, these findings emphasise the importance of balancing the design of the intra-module connections and the bolting assemblies to achieve an optimal force-transfer mechanism while ensuring that the hybrid IMCs fulfil their damage mitigation function. It is also noteworthy that there was no significant bending deformation or yielding of the steel reinforcing plates of the rubber bearings, supporting their resilience for continued reuse, provided that the permanent deformation of the rubber layers is also deemed acceptable.

4.2. Observations on plasticity and critical regions

In Fig. 16, the distribution of equivalent plastic strain (PEEQ) is utilised to evaluate the extent of irreversible deformation (damage) in the hybrid IMJs, with blue areas indicating regions of zero plastic damage. The results supported the test observations, confirming that the hybrid IMC effectively restricts the spread of permanent damage into the main framing members of the volumetric module. Instead, plastic strains remain highly localised within the intra-module connection region and at the corners of the stiffeners where stress concentrations occur.

Notably, the plots also illustrated plastic strain concentrations at the four corners of the circular access openings in the vertical plates of the module corner fittings. The distribution of these strains is characteristic of the Vierendeel bending mechanism, which is typical for members with circular web openings subjected to high shear forces. Although the weakened corner fittings plates were sufficiently thick to prevent failure, these findings emphasise the critical regions around the access openings that require special attention to ensure the robustness of the corner fittings.

The parametric results indicate that the use of stiffeners has contrasting effects depending on the bolting assembly material. For specimens with SMA studs, adding stiffeners reduced the maximum equivalent plastic strain at ±3 % drift ratio, from approximately 6.8 % to 5.1 % in the positive loading direction and from 12 % to 7.5 % in the

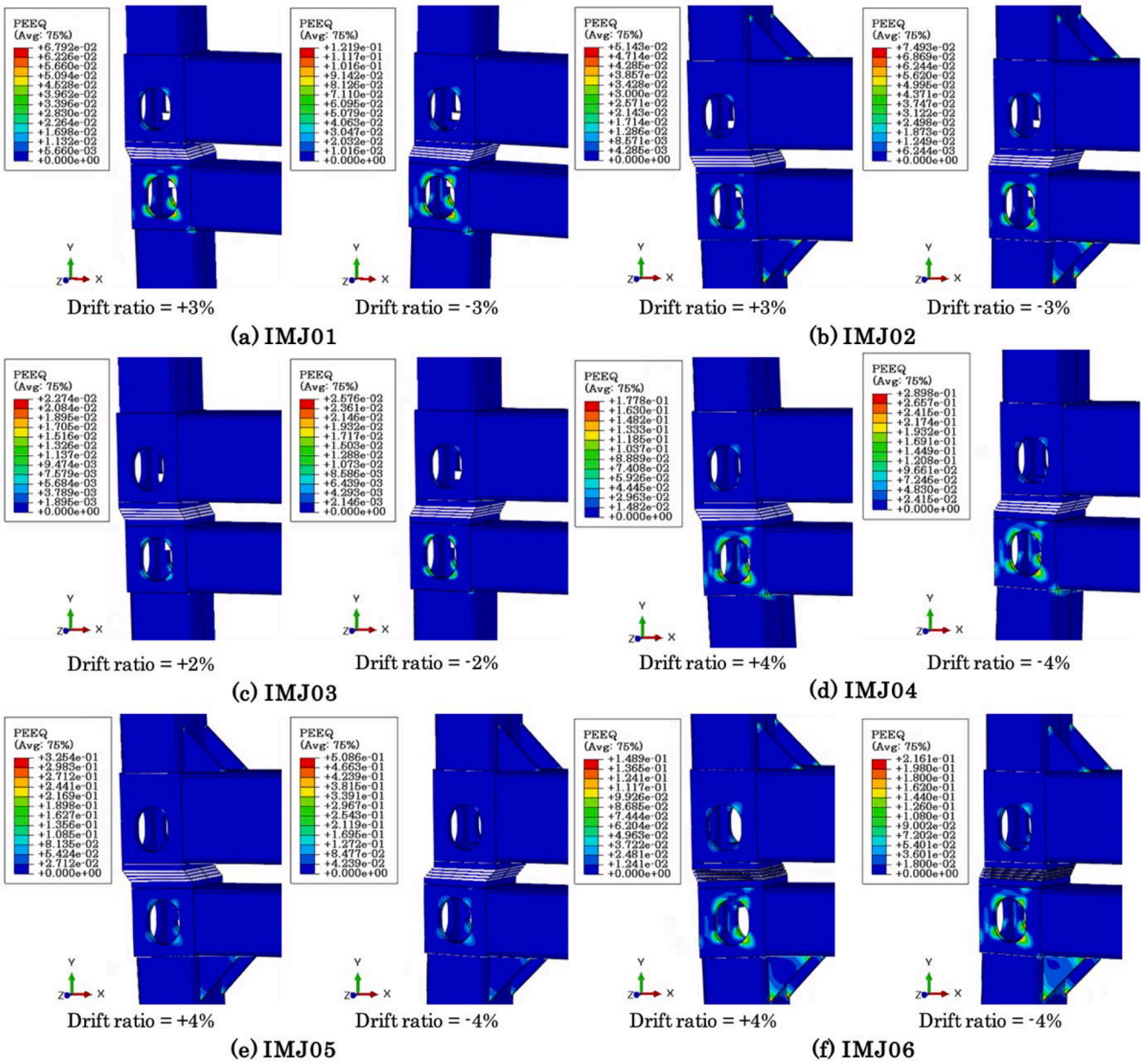

Fig. 16. Equivalent plastic strain (PEEQ) distribution of the joint members.

negative direction. In contrast, for specimens with standard high-strength steel (HSS) bolts, stiffeners increased the plastic strain demand at ±4 % drift ratio, with values rising from 17.8 % to 32.5 % (positive) and from 28.9 % to 50.9 % (negative).

Compared to the unstiffened M24 configuration, increasing the bolt diameter to M27 and adding stiffeners together helped reduce the peak plastic strain, from 18.8 % to 14.9 % in the positive direction and from 29.0 % to 21.6 % in the negative direction. These equivalent plastic strain (PEEQ) values must be interpreted with caution: the PEEQ measure does not apply to the superelastic material model used for the SMA studs. Therefore, for IMJ01–IMJ03, the PEEQ plots reflect plastic strain only in the surrounding steel parts, whereas for IMJ04–IMJ06 they include the HSS bolts as well.

Fig. 17 shows that using an HSS bolt (b) instead of an SMA stud (a) slightly reduced the peak equivalent plastic strain in the surrounding steel parts: from 6.8 % to 4.8 % in the positive loading direction and from 12.2 % to 9.6 % in the negative direction at ±3 % drift ratio. However, the PEEQ plots for the SMA configuration do not capture the superelastic behaviour of the Ni–Ti alloy itself but only the plasticity in the adjacent steel components. In both cases, localised plastic strain peaks occur mainly around the access hole edges and, for the HSS bolt, in the bolt shank under reverse loading.

This comparison highlights that the amount of plasticity developed in the joint is governed more by bolt size and joint detailing than by bolt material alone. The SMA stud's key benefit lies in its superelastic re-centring capability and its reduced tendency for permanent deformation, which can greatly facilitate post-earthquake demountability. In contrast, HSS bolts may become severely bent, complicating disassembly and reuse. Properly sized HSS bolts remain a practical alternative when combined with thoughtful joint detailing.

Overall, these findings emphasise the importance of balancing bolt dimensions and connection stiffness to achieve reliable seismic performance and maintain the ease of module disassembly for future reuse.

4.3. Stress and strain distribution in the rubber bearings

A detailed investigation was conducted to analyse the stresses and strains developed in the rubber bearing at various critical stages throughout the test. Specimen IMJ06 was selected for this in-depth analysis, while the observations discussed are relevant for the rest of specimens as well, which exhibited the same type of behaviour differing only in specific stress and strain levels. The true (Cauchy) stresses (S) defined as force per current area and logarithmic strains (LE) were used to plot the contours in Fig. 18, where the positive values indicate tension. Logarithmic strains were preferred over nominal (engineering) strains (NE) due to their improved accuracy for geometrically non-linear, large-strain analysis of hyperelastic materials, such as the present constitutive model used for high-damping rubber.

Fig. 18 (a) illustrates the compressive stresses (S22) and strains (LE22) and the shear stresses (S12) and strains (LE12) developed in the rubber layers subjected to the 100 kN axial load. While the global compressive stress in the bearing matched the analytical prediction obtained by dividing the vertical force by the cross-sectional area of the rubber bearing (4.7 MPa), the results also revealed two vertical struts of higher compressive stress, up to 7.2 MPa, located midway between the inner hole and outside face of the bearing. Local tensile stresses and strains were developed in the extremities of the rubber layers along the bulging areas, with high shear stresses and strains concentrated at opposite corners near the edges of each rubber layer.

Under axial load and horizontal shear (Fig. 18 (b)), diagonal compression struts were formed on the side of the bearing opposite to the loading direction, with tension developed on the opposite sides. The FE results showed that the logarithmic shear strains were in good agreement with the analytically predicted 80 % shear strain reported in [43] for a large portion of each rubber layer. However, the analysis also revealed significantly higher shear strains, ranging from two to four times larger, concentrated at the corners of each rubber layer. These stress concentrations were due to the constraint provided by the bonded steel reinforcing plates, underscoring the importance of ensuring the quality of the rubber-to-metal bond to prevent premature failure by delamination in these highly stressed regions.

These observations were consistent with the findings reported in the literature [69–71], supporting the accuracy of the present FE model in capturing the typical behaviour of rubber bearings subjected to axial load and horizontal shear.

4.4. Evolution of stress distribution in the bolting assemblies

Fig. 19 shows the stress state in the SMA stud at critical stages during the cyclic load sequence, providing insights into the force transfer mechanism developed by the hybrid IMC up to the failure of the bolting assembly observed during testing. While the results are presented for specimen IMJ01, they remain highly representative for all other specimens, as the tests revealed consistent deformation and failure modes characterised by bending of the bolts.

Overall, the FEA results aligned with the experimental observations, confirming the low stress levels developed by the bolting assembly up to 0.5 % drift ratio. The stress levels nearly doubled during the 0.75 % drift ratio as the bolting assembly experienced more pronounced bending deformation due to the increasing horizontal shear in the hybrid IMC.

According to the stress contours in Fig. 19, the forward transformation start stress $\sigma_{Ms} = 525$ N/mm^2 was first reached during the +1 % drift ratio cycle, indicating that the initial linear elastic stage was exceeded in certain regions at the base of the transition zone in the SMA stud. The forward transformation finish stress $\sigma_{Ms} = 610$ N/mm^2 was first reached during the reverse loading at 2 % drift ratio, signalling that

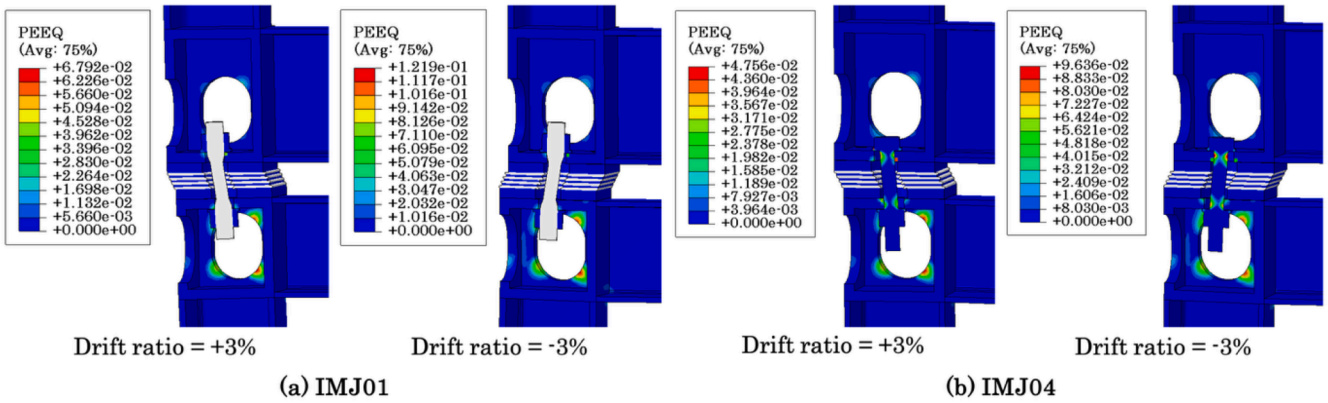

Fig. 17. PEEQ comparison between the unstiffened specimens with SMA studs (M20–27) and HSS bolts (M24) at ±3 % drift ratio.

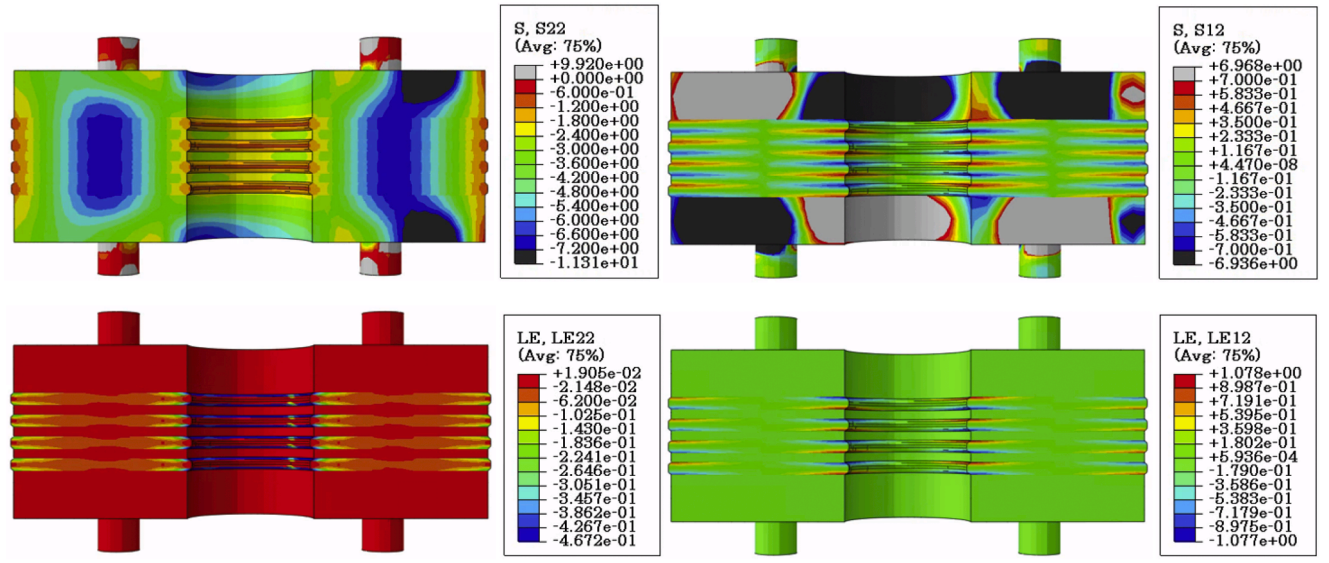

(a) Stress and strain in rubber bearing under 100 kN axial load

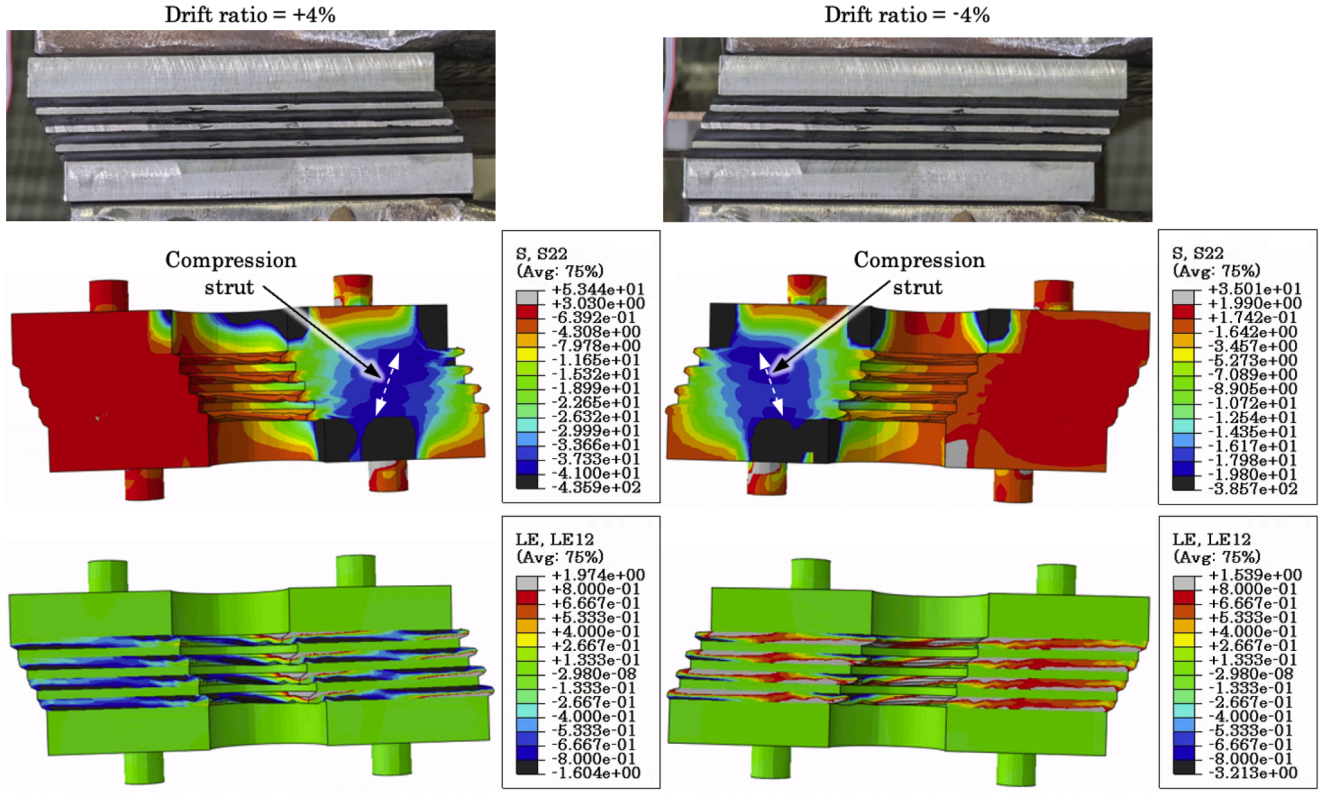

(b) Stress and strain in rubber bearing at 4% drift ratio

Fig. 18. Deformation, stress, and strain distribution in the rubber bearings.

the superelastic limit was exceeded in the SMA stud. Finally, the stress developed in the SMA stud during the -3 % drift ratio cycle (failure in the tests) suggested that the ultimate tensile strength of the austenitic Ni-Ti alloy was approximately 1370 N/mm^2, which is consistent with the typical range of 895 N/mm^2 to 1900 N/mm^2 provided by Fang and Wang [72].

5. Concluding remarks

This study investigated the cyclic behaviour of a novel hybrid inter-module connection (HyMC™) designed to enhance the seismic resilience of steel modular buildings. A high-fidelity finite element (FE) model was developed to validate and complement earlier experimental work, providing insights into the force-transfer mechanisms and stress distribution within the connection components. The FEA demonstrated a strong correlation with the test data in terms of stiffness, strength, and overall hysteretic behaviour, confirming the model's ability to capture the structural response under cyclic lateral loading.

The analysis revealed that stress concentrations were primarily located at the intra-module connections, aligning with observed failure

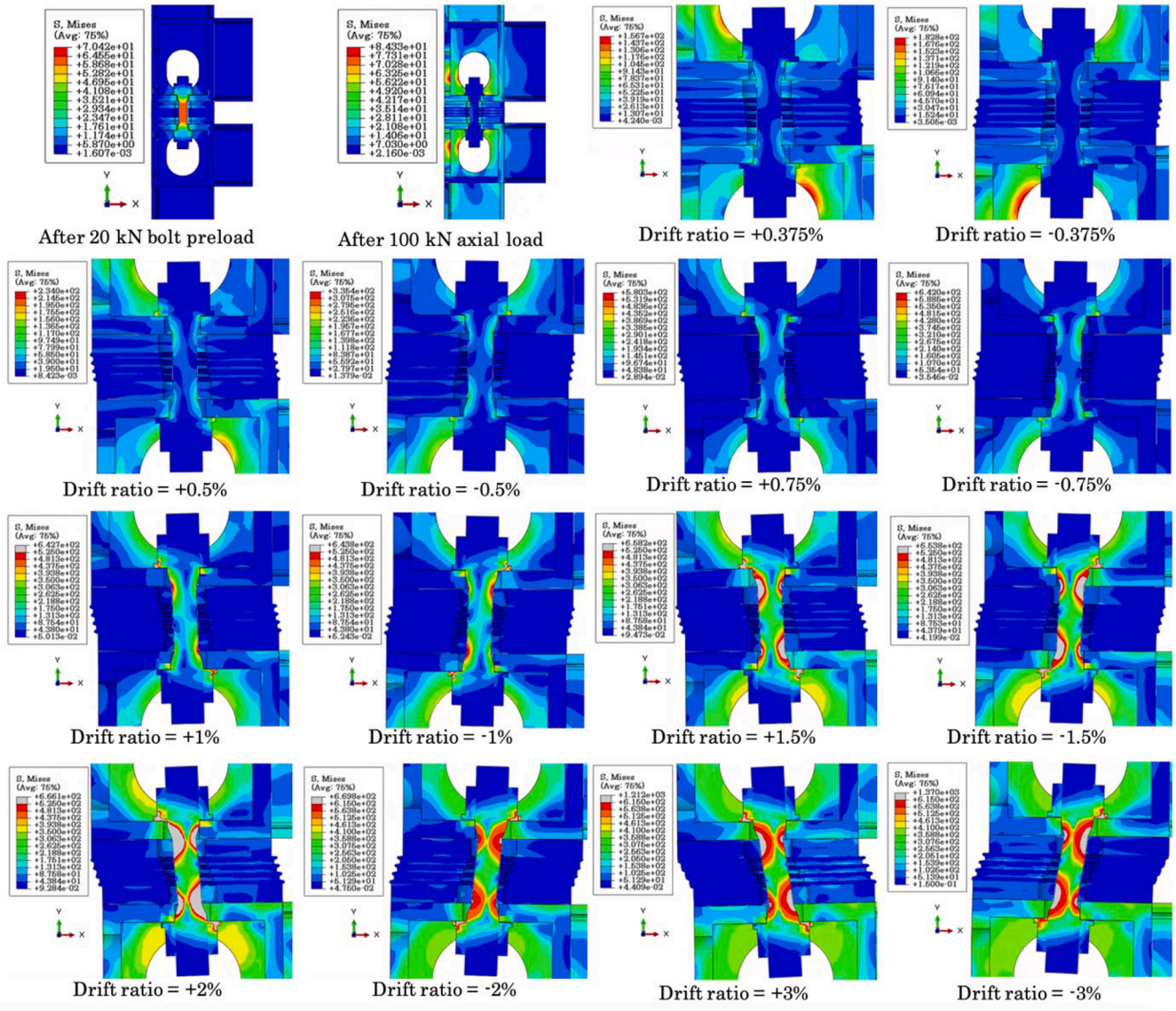

Fig. 19. Stress development in the bolting assembly (shown for specimen IMJ01).

patterns in past experiments. The inclusion of stiffeners in these connections effectively redistributed stress away from the beam-column joint zone but led to increased stresses in the bolting assemblies.

The stress response of the bolting assembly evolved as cyclic loading progressed, with initially low stress levels increasing significantly as deformation demands grew. In particular, the forward transformation start stress in the SMA studs was reached at relatively small drift ratios (±1 % drift ratio), indicating that superelastic deformation contributed to the connection's response. However, further cycles led to higher stresses, with the forward transformation finish stress exceeded at larger drift levels (>2 % drift ratio), suggesting that the bolts experienced increasing plasticity and loss of stiffness.

Comparisons with high-strength steel (HSS) bolts highlight that bolt size and joint detailing play a more decisive role than bolt material alone in controlling stress concentrations and plastic strain spread within the connection. While increasing the bolt diameter effectively reduced stress levels, the superelastic properties of SMA studs provide an added benefit by promoting re-centring and facilitating post-earthquake demountability. In contrast, HSS bolts are more prone to permanent bending, which could complicate disassembly and reuse. These findings underscore the importance of balancing geometric design, such as appropriate bolt sizing and stiffener use, with material choice to achieve robust seismic performance and support the reuse of modular units.

The rubber bearing component performed as expected under compression and shear, though higher stress concentrations were observed at the corners of the rubber layers, highlighting the importance of ensuring a strong rubber-to-metal bond to prevent premature failure.

Overall, the findings reinforce the effectiveness of the hybrid IMC in limiting the spread of permanent damage in the framing elements of the volumetric modules, particularly through the combined contribution of the rubber bearings and bolting assembly in resisting lateral loads. The proposed connection offers a promising step toward improving the seismic resilience and reusability of modular buildings, supporting the broader goal of sustainable, damage-resistant, and reconfigurable construction.

Future work should focus on refining the hybrid IMC design through parametric FE studies to optimise its geometry and in some cases the material selection, to enhance the connection's energy dissipation capacity, re-centring capability, and thus overall seismic performance. Numerical studies should also be extended to edge joints where four modules meet, to facilitate the development of accurate simplified joint models for global analysis. Future studies should also investigate the use

of anti-vibration fasteners with controlled preloads to enhance the slip resistance and overall reliability of the connection under cyclic loading.

Author agreement statement

We the undersigned declare that this manuscript is original, has not been published before and is not currently being considered for publication elsewhere.

We confirm that the manuscript has been read and approved by all named authors and that there are no other persons who satisfied the criteria for authorship but are not listed. We further confirm that the order of authors listed in the manuscript has been approved by all of us.

We understand that the Corresponding Author is the sole contact for the Editorial process. He/she is responsible for communicating with the other authors about progress, submissions of revisions and final approval of proofs

CRediT authorship contribution statement

Dan-Adrian Corfar: Writing – original draft, Visualization, Methodology, Investigation, Formal analysis, Data curation, Conceptualization. **Konstantinos Daniel Tsavdaridis:** Writing – review & editing, Validation, Supervision, Software, Resources, Project administration, Methodology, Investigation, Funding acquisition, Conceptualization.

Declaration of competing interest

The authors declare that they have no known competing financial interests or personal relationships that could have appeared to influence the work reported in this paper.

Acknowledgements

This work is funded by the Engineering and Physical Sciences Research Council (EPSRC) in the UK and the industrial partner SC4 (UK) Limited. The authors would also like thank the Leverhulme Trust (Royal Academy of Engineering) for their initial financial support.

Data availability

No data was used for the research described in the article.

References

[1] E. Prasher, Prefabrication in ancient period, IOSR 01 (2016) 34–39, https://doi.org/10.9790/1684-15010010134-39.
[2] R.M. Lawson, R.G. Ogden, C. Goodier, Design in Modular Construction, CRC Press, Oxon, 2014.
[3] HM Government, The Construction Playbook. Government Guidance On Sourcing and Contracting Public Works Projects and Programmes, HM Government, 2022.
[4] C. Goodier, A. Gibb, Future opportunities for offsite in the UK, Constr. Manag. Econ. 25 (2007) 585–595, https://doi.org/10.1080/01446190601071821.
[5] W. Ferdous, A. Manalo, A. Sharda, Y. Bai, T.D. Ngo, P. Mendis, Construction industry transformation through modular methods, Eds., in: S.H. Ghaffar, P. Mullett, E. Pei, J. Roberts (Eds.), Innovation in Construction, Springer, Cham, 2022, pp. 259–276, https://doi.org/10.1007/978-3-030-95798-8_11.
[6] C. Chen, Advantages and barriers of modular construction method in constructing buildings, Proc. Inst. Civ. Eng. - Smart Infrastruct. Constr. 176 (2023) 75–84, https://doi.org/10.1680/jsmic.22.00017.
[7] J.R. McConnell, L.A. Fahnestock, Innovations in steel design: research needs for global sustainability, J. Struct. Eng. 141 (2015) 02514001, https://doi.org/10.1061/(ASCE)ST.1943-541X.0001185.
[8] R. Minunno, T. O'Grady, G.M. Morrison, R.L Gruner, Exploring environmental benefits of reuse and recycle practices: a circular economy case study of a modular building, Resour. Conserv. Recycl. 160 (2020), https://doi.org/10.1016/j.resconrec.2020.104855.
[9] E. Iacovidou, P. Purnell, K.D. Tsavdaridis, K. Poologanathan, Digitally enabled modular construction for promoting modular components reuse: a UK view, J. Build. Eng. 42 (2021) 102820, https://doi.org/10.1016/j.jobe.2021.102820.
[10] Z.W. Sajid, F. Ullah, S. Qayyum, R. Masood, Climate change mitigation through modular construction, Smart Cities 7 (2024) 566–596, https://doi.org/10.3390/smartcities7010023.
[11] United Nations, Department of Economic and Social Affairs, Population Division, World Urbanization Prospects: The 2018 Revision, United Nations, New York, 2019.
[12] M. Pesaresi, D. Ehrlich, T. Kemper, A. Siragusa, A. Florczyk, S. Freire, et al., Atlas of the Human Planet 2017: Global Exposure to Natural Hazards, Publications Office of the European Union: European Commission, 2017.
[13] C. He, Q. Huang, X. Bai, D.T. Robinson, P. Shi, Y. Dou, et al., A global analysis of the relationship between urbanization and fatalities in earthquake-prone areas, Int J Disaster Risk Sci 12 (2021) 805–820, https://doi.org/10.1007/s13753-021-00385-z.
[14] United Nations, Department of Economic and Social Affairs, Transforming Our World: The 2030 Agenda for Sustainable Development, United Nations, 2015.
[15] FEMA, NEHRP Guidelines for the Seismic Rehabilitation of Buildings, Federal Emergency Management Agency, Applied Technology Council, Washington, D.C, 1997.
[16] Deierlein G., Krawinkler H., Cornell C.A. A framework for performance-based earthquake engineering, 2003.
[17] M.J.N. Priestley, Performance based seismic design, in: Proceedings of the 12th World Conference on Earthquake Engineering, Auckland, New Zealand, 2000, pp. 325–346.
[18] A. Ghobarah, Performance-based design in earthquake engineering: state of development, Eng. Struct. 23 (2001) 878–884, https://doi.org/10.1016/S0141-0296(01)00036-0.
[19] M. Bruneau, S.E. Chang, R.T. Eguchi, G.C. Lee, T.D. O'Rourke, A.M. Reinhorn, et al., A framework to quantitatively assess and enhance the seismic resilience of communities, Earthq. Spectra 19 (2003) 733–752, https://doi.org/10.1193/1.1623497.
[20] H. Hao, K. Bi, W. Chen, T.M. Pham, J. Li, Towards next generation design of sustainable, durable, multi-hazard resistant, resilient, and smart civil engineering structures, Eng. Struct. 277 (2023) 115477, https://doi.org/10.1016/j.engstruct.2022.115477.
[21] G. Tsionis, Seismic Resilience – Concept, Metrics and Integration With Other Hazards, Publications Office of the European Union, Luxembourg, 2014, https://doi.org/10.2788/713724.
[22] E.-F. Deng, L. Zong, Y. Ding, Z. Zhang, J.-F. Zhang, F.-W. Shi, et al., Seismic performance of mid-to-high rise modular steel construction - a critical review, Thin-Walled Struct. 155 (2020) 106924, https://doi.org/10.1016/j.tws.2020.106924.
[23] D.-A. Corfar, K.D. Tsavdaridis, A comprehensive review and classification of inter-module connections for hot-rolled steel modular building systems, J. Build. Eng. 50 (2022) 104006, https://doi.org/10.1016/j.jobe.2022.104006.
[24] Z. Chen, J. Liu, Y. Yu, Experimental study on interior connections in modular steel buildings, Eng. Struct. 147 (2017) 625–638, https://doi.org/10.1016/j.engstruct.2017.06.002.
[25] Z. Chen, J. Liu, Y. Yu, C. Zhou, R. Yan, Experimental study of an innovative modular steel building connection, J. Constr. Steel Res. 139 (2017) 69–82, https://doi.org/10.1016/j.jcsr.2017.09.008.
[26] E.-F. Deng, L. Zong, Y. Ding, X.-M. Dai, N. Lou, Y. Chen, Monotonic and cyclic response of bolted connections with welded cover plate for modular steel construction, Eng. Struct. 167 (2018) 407–419, https://doi.org/10.1016/j.engstruct.2018.04.028.
[27] E.-F. Deng, L. Zong, Y. Ding, Y.-B. Luo, Seismic behavior and design of cruciform bolted module-to-module connection with various reinforcing details, Thin-Walled Struct. 133 (2018) 106–119, https://doi.org/10.1016/j.tws.2018.09.033.
[28] R. Sanches, O. Mercan, B. Roberts, Experimental investigations of vertical post-tensioned connection for modular steel structures, Eng. Struct. 175 (2018) 776–789, https://doi.org/10.1016/j.engstruct.2018.08.049.
[29] Y. Wang, J. Xia, R. Ma, B. Xu, T. Wang, Experimental study on the flexural behavior of an innovative modular steel building connection with installed bolts in the columns, Appl. Sci. 9 (2019), https://doi.org/10.3390/app9173468.
[30] Z. Chen, J. Wang, J. Liu, K. Khan, Seismic behavior and moment transfer capacity of an innovative self-locking inter-module connection for modular steel building, Eng. Struct. 245 (2021) 112978, https://doi.org/10.1016/j.engstruct.2021.112978.
[31] R. Ma, J. Xia, H. Chang, B. Xu, L. Zhang, Experimental and numerical investigation of mechanical properties on novel modular connections with superimposed beams, Eng. Struct. 232 (2021), https://doi.org/10.1016/j.engstruct.2021.111858.
[32] S.-Y. Zhai, Y.-F. Lyu, K. Cao, G.-Q. Li, W.-Y. Wang, C. Chen, Experimental study on bolted-cover plate corner connections for column-supported modular steel buildings, J. Constr. Steel Res. 189 (2022) 107060, https://doi.org/10.1016/j.jcsr.2021.107060.
[33] S. Lee, J. Park, S. Shon, C. Kang, Seismic performance evaluation of the ceiling-bracket-type modular joint with various bracket parameters, J. Constr. Steel Res. 150 (2018) 298–325, https://doi.org/10.1016/j.jcsr.2018.08.008.
[34] B.-H. Cho, J.-S. Lee, H. Kim, D.-J. Kim, Structural performance of a new blind-bolted frame modular beam-column connection under lateral loading, Appl. Sci. 9 (2019), https://doi.org/10.3390/app9091929.
[35] X.-M. Dai, L. Zong, Y. Ding, Z.-X. Li, Experimental study on seismic behavior of a novel plug-in self-lock joint for modular steel construction, Eng. Struct. 181 (2019) 143–164, https://doi.org/10.1016/j.engstruct.2018.11.075.
[36] S.-S. Lee, K.-S. Park, J.-S. Jung, K.-S. Lee, Evaluation of the Structural Performance of a Novel Methodology for Connecting Modular Units Using Straight and Cross-Shaped Connector Plates in Modular Buildings, Appl. Sci. 10 (2020) 8186, https://doi.org/10.3390/app10228186.

[37] S.-Y. Zhai, Y.-F. Lyu, K. Cao, G.-Q. Li, W.-Y. Wang, C. Chen, Seismic behavior of an innovative bolted connection with dual-slot hole for modular steel buildings, Eng. Struct. 279 (2023) 115619, https://doi.org/10.1016/j.engstruct.2023.115619.
[38] C. Yang, H. Chen, H. Wen, Q. Wang, B. Zhang, J. Ou, Experimental study on seismic performance of internal cruciform joints of grouting sleeve connection for modular integrated construction, Eng. Struct. 301 (2024) 117325, https://doi.org/10.1016/j.engstruct.2023.117325.
[39] P. Sultana, M.A. Youssef, Seismic performance of modular steel-braced frames utilizing superelastic shape memory alloy bolts in the vertical module connections, J. Earthq. Eng. 24 (2018) 628–652, https://doi.org/10.1080/13632469.2018.1453394.
[40] J. Jing, G.C. Clifton, K. Roy, J.B.P. Lim, Seismic protection of modular buildings with galvanised steel wall tracks and bonded rubber units: experimental and numerical study, Thin-Walled Struct. 162 (2021), https://doi.org/10.1016/j.tws.2021.107563.
[41] S.V. Sendanayake, D.P. Thambiratnam, N.J. Perera, T.H.T. Chan, S. Aghdamy, Enhancing the lateral performance of modular buildings through innovative inter-modular connections, Structures 29 (2021) 167–184, https://doi.org/10.1016/j.istruc.2020.10.047.
[42] D.-A. Corfar, K.D. Tsavdaridis, A hybrid inter-module connection for steel modular building systems with SMA and high-damping rubber components, Eng. Struct. 289 (2023) 116281, https://doi.org/10.1016/j.engstruct.2023.116281.
[43] D.-A. Corfar, K.D. Tsavdaridis, Testing novel hybrid inter-module joints for steel modular buildings under cyclic load, Eng. Struct. 315 (2024) 118495, https://doi.org/10.1016/j.engstruct.2024.118495.
[44] K.D. Tsavdaridis, D.-A. Corfar, Insights Into the Cyclic Behaviour of Novel Hybrid Inter-Module Joints Under Lateral Load, 2024. Rio de Janeiro, Brazil.
[45] BSI, Eurocode 3: Design of Steel Structures - Part 1-8: Design of Joints, BSI, London, 2010.
[46] B. Xu, J. Xia, H. Chang, R. Ma, L. Zhang, Experimental and numerical investigation on the lateral force resistance of modular steel sub-frames with laminated double beam, J. Build. Eng. 46 (2022) 103666, https://doi.org/10.1016/j.jobe.2021.103666.
[47] B. Xu, J. Xia, H. Chang, R. Ma, L. Zhang, Evaluation of superimposed bending behaviour of laminated channel beams in modular steel buildings subjected to lateral load, Thin-Walled Struct. 175 (2022) 109234, https://doi.org/10.1016/j.tws.2022.109234.
[48] B. Xu, J. Xia, R. Ma, H. Chang, C. Yang, L. Zhang, Investigation on interfacial slipping response of laminated channel beams with bolt connections in modular steel buildings, J. Build. Eng. 63 (2023) 105441, https://doi.org/10.1016/j.jobe.2022.105441.
[49] B. Xu, J. Xia, H. Chang, X. Chen, C. Yang, L. Zhang, Numerical-analytical investigation on bending performance of laminated beams in modular steel buildings, J. Constr. Steel Res. 217 (2024) 108630, https://doi.org/10.1016/j.jcsr.2024.108630.
[50] R.M. Lawson, R.G. Ogden, R. Bergin, Application of modular construction in high-rise buildings, J. Archit. Eng. 18 (2012) 148–154, https://doi.org/10.1061/(asce)ae.1943-5568.0000057.
[51] A.N. Alagha, S. Hussain, W. Zaki, Additive manufacturing of shape memory alloys: a review with emphasis on powder bed systems, Mater. Des. 204 (2021) 109654, https://doi.org/10.1016/j.matdes.2021.109654.
[52] L. Xue, K.C. Atli, C. Zhang, N. Hite, A. Srivastava, A.C. Leff, et al., Laser powder bed fusion of defect-free niti shape memory alloy parts with superior tensile superelasticity, Acta Mater. 229 (2022) 117781, https://doi.org/10.1016/j.actamat.2022.117781.
[53] K. Kubášová, V. Drátovská, M. Losertová, P. Salvetr, M. Kopelent, F. Kořínek, et al., A review on additive manufacturing methods for niti shape memory alloy production, Materials 17 (2024) 1248, https://doi.org/10.3390/ma17061248.
[54] C. Fang, SMAs for infrastructures in seismic zones: a critical review of latest trends and future needs, J. Build. Eng. 57 (2022) 104918, https://doi.org/10.1016/j.jobe.2022.104918.
[55] Dassault Systèmes SIMULIA Corp. Abaqus CAE (2024) 2024.
[56] A.W. Lacey, W. Chen, H. Hao, Experimental methods for inter-module joints in modular building structures – A state-of-the-art review, J. Build. Eng. 46 (2022) 103792, https://doi.org/10.1016/j.jobe.2021.103792.
[57] AISC, Seismic Provisions for Structural Steel Buildings, American Institute of Steel Construction, Chicago, 2022.
[58] SAC Joint Venture, Recommended Seismic Design Criteria for New Steel Moment-Frame Buildings, Federal Emergency Management Agency, 2000.
[59] BSI, Eurocode 3: Design of Steel Structures - Part 1-1: General rules and Rules For Buildings, BSI, London, 2023.
[60] F. Auricchio, R.L. Taylor, Shape-memory alloys: modelling and numerical simulations of the finite-strain superelastic behavior, Comput. Methods Appl. Mech. Eng. 143 (1997) 175–194, https://doi.org/10.1016/S0045-7825(96)01147-4.
[61] F. Auricchio, R.L. Taylor, J. Lubliner, Shape-memory alloys: macromodelling and numerical simulations of the superelastic behavior, Comput. Methods Appl. Mech. Eng. 146 (1997) 281–312, https://doi.org/10.1016/S0045-7825(96)01232-7.
[62] M.A. Farmani, M. Ghassemieh, Steel beam-to-column connections equipped with SMA tendons and energy dissipating devices including shear tabs or web hourglass pins, J. Constr. Steel Res. 135 (2017) 30–48, https://doi.org/10.1016/j.jcsr.2017.04.003.
[63] C. Fang, M.C.H. Yam, T.-M. Chan, W. Wang, X. Yang, X. Lin, A study of hybrid self-centring connections equipped with shape memory alloy washers and bolts, Eng. Struct. 164 (2018) 155–168, https://doi.org/10.1016/j.engstruct.2018.03.006.
[64] B. Wang, M. Nishiyama, S. Zhu, M. Tani, H. Jiang, Development of novel self-centering steel coupling beams without beam elongation for earthquake resilience, Eng. Struct. 232 (2021), https://doi.org/10.1016/j.engstruct.2020.111827.
[65] H.D. Nguyen, E. Choi, S.-N. Nguyen, T.-K. Pham, Performance of self-centering devices containing superelastic SMA bars and their application via finite element analysis, Eng. Struct. 237 (2021) 112113, https://doi.org/10.1016/j.engstruct.2021.112113.
[66] S.S. Askariani, S. Garivani, I. Hajirasouliha, N. Soleimanian, Innovative self-centering systems using shape memory alloy bolts and energy dissipating devices, J. Constr. Steel Res. 190 (2022) 107127, https://doi.org/10.1016/j.jcsr.2021.107127.
[67] C. Qiu, J. Liu, X. Du, Cyclic behavior of SMA slip friction damper, Eng. Struct. 250 (2022) 113407, https://doi.org/10.1016/j.engstruct.2021.113407.
[68] J. Chen, W. Wang, C. Fang, Manufacturing, testing and simulation of novel SMA-based variable friction dampers with enhanced deformability, J. Build. Eng. 45 (2022) 103513, https://doi.org/10.1016/j.jobe.2021.103513.
[69] J.M. Kelly, Earthquake-Resistant Design with Rubber, Springer London, London, 1997, https://doi.org/10.1007/978-1-4471-0971-6.
[70] K.N. Kalfas, S.A. Mitoulis, K. Katakalos, Numerical study on the response of steel-laminated elastomeric bearings subjected to variable axial loads and development of local tensile stresses, Eng. Struct. 134 (2017) 346–357, https://doi.org/10.1016/j.engstruct.2016.12.015.
[71] A. Orfeo, E. Tubaldi, A.H. Muhr, D. Losanno, Mechanical behaviour of rubber bearings with low shape factor, Eng. Struct. 266 (2022) 114532, https://doi.org/10.1016/j.engstruct.2022.114532.
[72] C. Fang, W. Wang, Shape Memory Alloys For Seismic Resilience, Springer, Singapore, 2020.